A Appendix - Benchmark of Creep-SCLAY1S model viscous response

In order to benchmark the viscous response of the Creep-SCLAY1S model with a given parameter set, comparison of model response to empirical strain rate dependency have been made at element level. Comparisons are made with respect to rate-dependency of apparent preconsolidation pressure and undrained shear strength.

The model parameter set for the simulations was initially that of the Göta tunnel case study, presented in Chapter 3. It can be noted that β in eq. 2.49, i.e. $\beta=(\lambda_i^*\text{-}\kappa^*)/\mu_i^*$ then equals (0.085-0.013)/0.0182=40. Following the isotache concept relating the effective stress state, the reference preconsolidation stress and the volumetric creep strain rate (Grimstad, Haji Ashrafi, et al. 2016). β is analogue but the inverse to the "rate parameter", B, described by Länsivaara (1999). B was found to be 0.06-0.07 by Länsivaara (1999) and Claesson (2003). This corresponds to β=14-17.

The modified creep index was altered to 1/250 and the results are also included. This results in β=(0.085-0.013)/0.004=18. Also included is the parameter set from an additional paper on modelling of Gothenburg clay (Petalas et al. 2019).

These results need further studies as to find model parameter sets that results in both correct creep strain rate (compared to that measured in the field) and the empirical (expected) strain rate dependency.

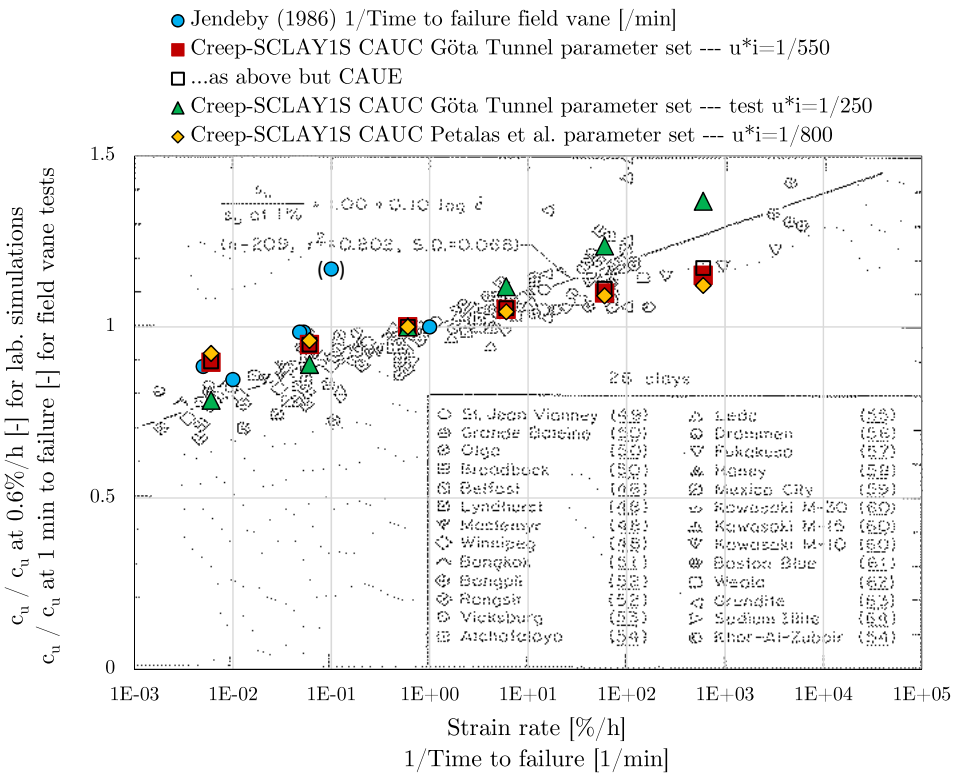

Figure A.1: *Benchmark of Creep-SCLAY1S model strain rate dependence of undrained shear strength. Model parameter sets according to Göta Tunnel case study and Petalas et al. (2019). Background data triaxial compression tests from Kulhawy and Mayne (1990).*

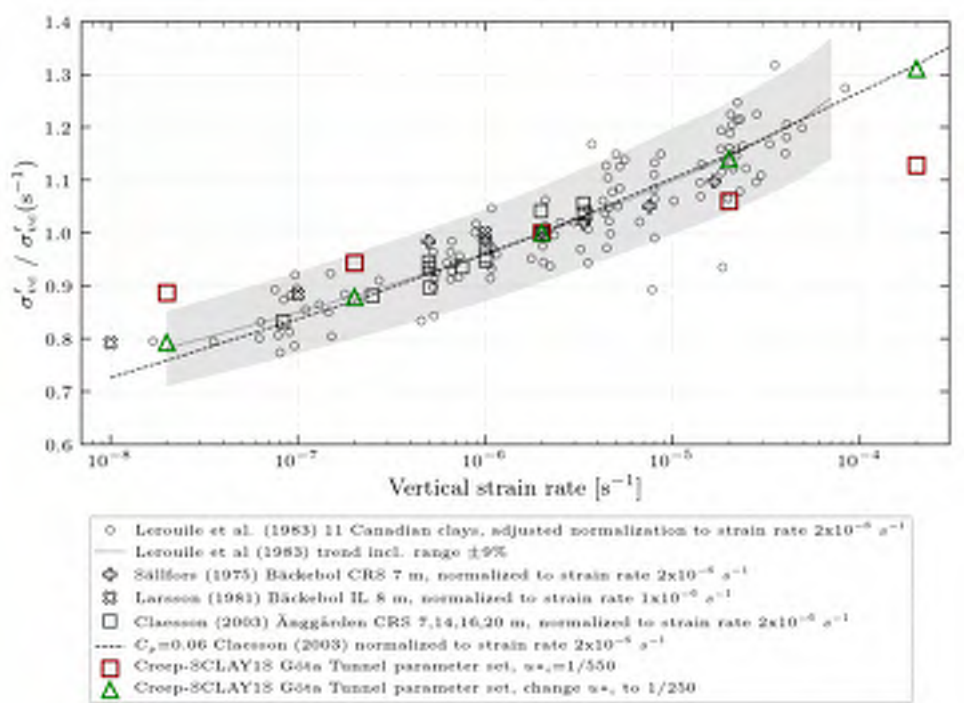

Figure A.2: *Benchmark of Creep-SCLAY1S model strain rate dependence of apparent preconsolidation pressure. Model parameter set according to Göta Tunnel case study.*

B Appendix - Case study Göta Tunnel

This appendix includes the paper draft of the case study analyses of Göta Tunnel contract J2. It is to be submitted to the journal Computers and Geotechnics in September 2020. The author of this report performed the calculations and wrote the paper. Co-authors Mats Karlsson, Anders Kullingsjö and Minna Karstunen assisted with comments on the writing. Initial analyses were presented at the European Conference on Soil Mechanics and Geotechnical Engineering in Reykjavik 2019 (Tornborg et al. 2019).

Title: Modelling the short- and long-term performance of Göta tunnel with a rate-dependent model for natural clays

Abstract: This paper presents the results from benchmarking of a rate-dependent constitutive soil model against the soil-structure response of a well instrumented excavation in soft sensitive clay: Göta Tunnel in Gothenburg. The excavation involved several stages with installation of sheet pile walls, piles, rock anchors and excavation carried underwater, followed by the construction of the permanent tunnel and backfill. The measurement data, which comprise of time-series of pore pressures, displacements, earth pressures and strut forces, provide valuable insights of the time-dependent response during the construction period (ca 3 years of monitoring). The long-term response is assessed using satellite data of current settlement rates in the area. The results demonstrate that the rate-dependent constitutive model for natural clays, referred to as Creep-SCLAY1S, is capable of capturing the measured response of pore pressures, earth pressures and strut forces over time, excluding the peak in the measurement values arising from pile and rock anchor installation, which was not explicitly modelled. The trends of vertical and horizontal displacements are captured well until the stage of dewatering, thereafter deformations continued to develop behind the sheet pile wall. This is considered to be attributed an effect of installation (drilling) of anchors and steel piles. The comparisons highlight the importance of assessing installation effects in the choice of construction methods, as well as the complexity and challenges in modelling of excavations in urban areas. It is further shown that a multitude of mechanisms will affect the soil response during construction works. These affect the resulting earth pressures acting against the retaining structure in the short-term, as well as against the permanent underground structures in the long-term.

B.1 Introduction

The increasing demand for infrastructure systems in urban areas, such as e.g. railway tunnels, underground water retention systems and deep basements, requires accurate predictions of earth pressures and deformations of the retaining structures to facilitate a design that is both safe and optimised. Optimisation is desirable for economical reasons, though rather more importantly, essential in order to minimise the environmental impact of construction. Predictions of the earth retaining structures are needed to optimise the structures for the short-term (construction period), considering both the safefy of the workers and the effects to nearby structures, as well as the long-term (design life time

of permanent structures) as part of asset management. Predictions need to account for characteristic clay properties such as e.g. rate-dependency (including effect of on-going creep settlements), anisotropy and destructuration of sensitive clay. Failure to incorporate the relevant features of the actual soil behaviour in geotechnical design may lead to sub optimised structures or at the extreme, severe failures such as those described by e.g. Magnus et al. (2005), Chen et al. (2015), and Do et al. (2016). However, as fundamental the concept of safety is to the design of excavations, deep excavations in close proximity to existing infrastructure in urban areas also coincide with strict regulations on the allowable deformations. Consequently, special assessment is required regarding how such restrictions effect the earth pressures acting on the retaining structures in the short-term as well as the long-term. Further, as the demand for deep(er) excavations and underground structures is increasing in urban areas, research is required to develop new calculation methods and to aid the implementation of the results into guidelines for design. Part of such research therefore includes benchmarking of advanced constitutive soil models against full scale field measurements.

Measurement data from a well instrumented excavation for a part of the Göta Tunnel in Gothenburg, Sweden, are revisited in this paper in order to benchmark an advanced contemporary constitutive soil model, Creep-SCLAY1S, which can incorporate many characteristic features of soft sensitive clay. The model has previously been benchmarked at element and field scale level in the case of embankment loading (Amavasai, Gras, et al. 2017; Amavasai, Sivasithamparam, et al. 2018). However, in order to adopt the soil model for excavation design, benchmarking of the model response is needed versus data from well instrumented excavations in soft clay. The aim of this paper is to study the measurement data from one such excavation for the Göta Tunnel. Results from numerical analyses are compared to unique measurement data of deformations, pore pressures, earth pressures and strut forces. The main focus of the study being on the time-dependent response during construction period, given that the measurement data cover ca 3 years of monitoring during this period, as well as the long-term performance supported by data from satellite measurements.

B.2 Site description

B.2.1 Site location and ground conditions

The Göta Tunnel was constructed from 2000-2006, partially as a cut-and-cover tunnel in soft clay deposits. The Göta Tunnel including the studied section, 1/430, is located in Central Gothenburg south of the Göta river, see Figure B.1. The studied part of the tunnel is located just North of Järntorget and a five storey building (Folkets hus) from the 1950s. A four storey building from the 1920s is located north-east of the the studied section. The geology of the Göta River valley is dominated by deep deposits of soft sensitive clay deposited during and after the last ice-age (glacial and post-glacial), reaching depths of maximum ca 100 m in Central Gothenburg. The deposits of soft clay in combination with considerable fill works, carried out mainly in the in the 19^{th} century in order to expand the city, has contributed to current on-going creep settlements within the city. The clay layer is assumed to be fully saturated. The ground level at

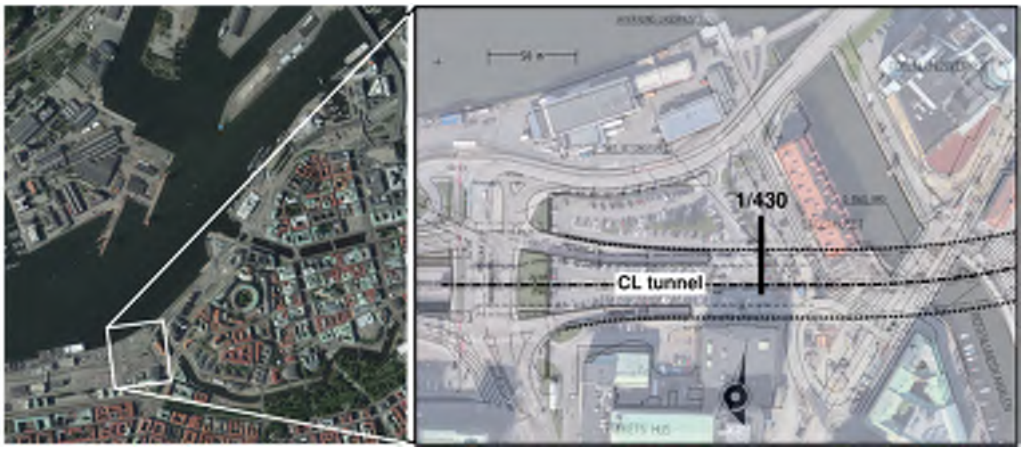

Figure B.1: *Overview of the part of Göta Tunnel just north of Järntorget in Central Gothenburg. The instrumented and studied section is highlighted including the centreline and extent of the tunnel.*

site corresponded to +12 (system RH2000) before excavation. The top soil layer consists of fill to approximately level +10. A layer of soft sensitive homogeneous clay is found down to approximately level -16, corresponding to ca 28 m depth below ground surface at the location of the sheet pile wall. Under this layer of clay there are some meters of friction material on top of the bedrock (granodiorite). Index properties of the clay layer in the studied section and an adjacent section (1/470) are presented in Figure B.2. The horizontal and vertical permeability of the clay at the site are assumed equal based on previous tests on Bäckebol clay (Larsson 1981) ca 10 km upstream the Göta River valley from the Göta Tunnel.

The overconsolidation ratio (OCR) varies from 1.1-1.4 in the studied section based on in-situ vertical effective stresses and preconsolidation pressures evaluated from undrained triaxial compression and CRS-oedometer tests. In an adjacent section, 1/470, OCR varies between 1.4-2.0. The high variability in OCR results from man-made induced variations in loading history. The higher values of OCR in the subarea of section 1/470 is due to the location of historic structures such as ware houses including storage of iron. The rate of settlement before construction works varied between 3-8 mm/year based on surveying of asphalt surfaces in the area around the studied part of the tunnel (Svahn and Liedberg 2001). Based on satellite data provided by the Swedish Transport Administration the current settlement rate just north of the tunnel varies between ca 2-6 mm/year, Figure B.3. As seen, the settlement rates varies within the city of Gothenburg due to the man-made loading history and constructions (e.g. old canals, harbour basins and piers) and Figure B.3 illustrates the challenges of construction in areas with on-going creep settlements.

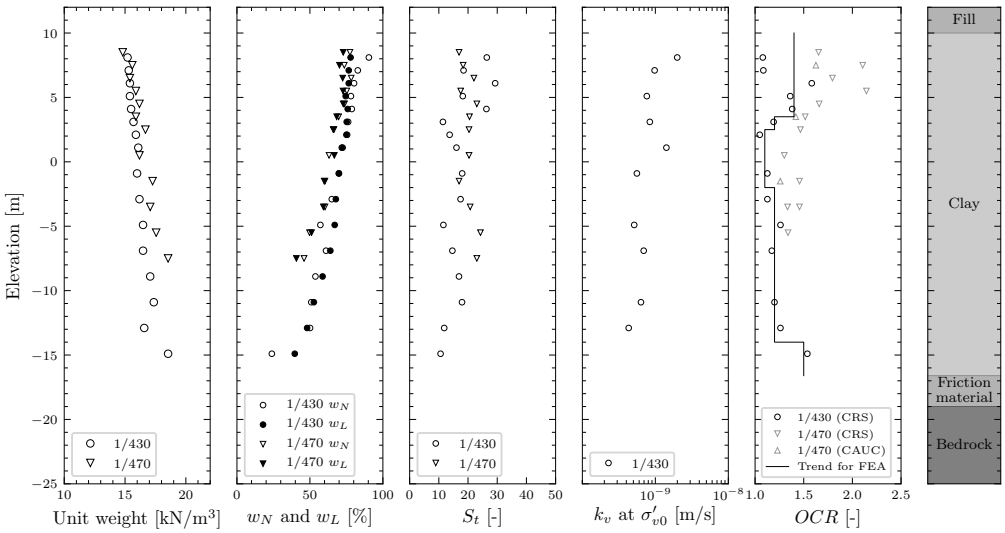

Figure B.2: *Soil profile and index properties of the clay layer.*

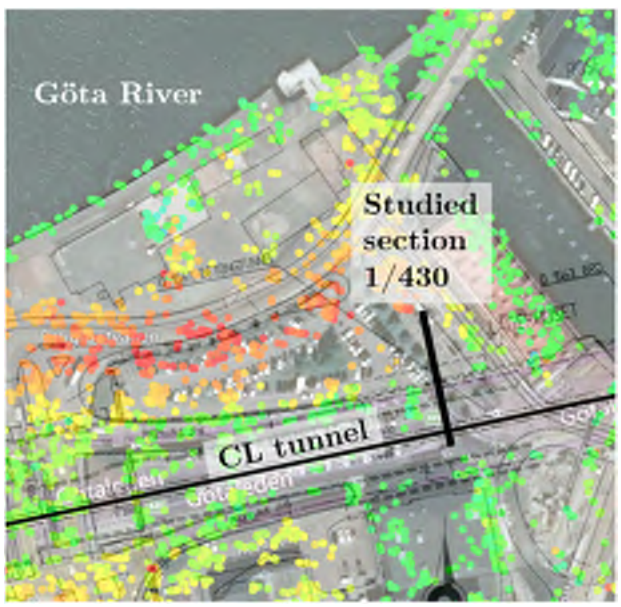

Figure B.3: *InSAR satellite data of current settlement rates in the area. Green=0 mm/year to red ≥10 mm/year (image courtesy of the Swedish Transport Administration).*

B.2.2 The permanent structure

An cross section of the tunnel structure is presented in Figure B.4. The tunnel comprise of a main structure divided by a continuous centerline column. The main tunnel, width 24 m, is in the studied section complemented by additional ramp segments extending the total width to 40 m. The foundation contains rows of 0.4×0.4 m^2 pre-cast concrete displacement piles which were hammered down to firm friction material in an out-of-plane center to center (cc) distance varying between 2.0-2.5 m.

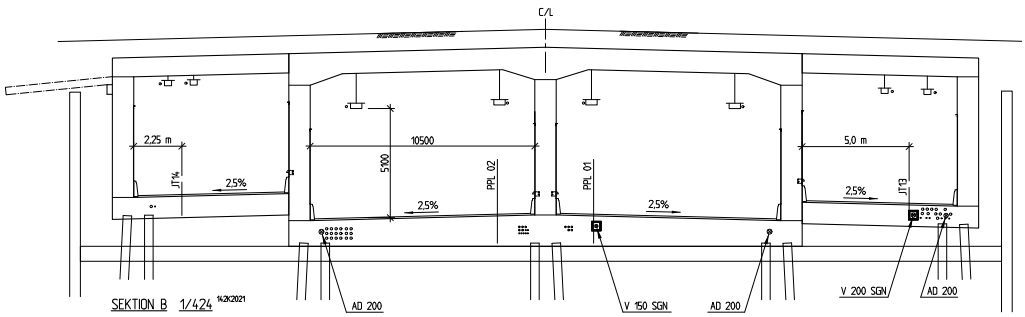

Figure B.4: *Approximately north (left in picture) to south section through the tunnel.*

B.2.3 Earth retaining structure and construction sequence

The design of the earth retaining system was made by the contractors independent analyses. The excavation was carried out within steel sheet pile walls (SPW) of profile AZ36 (steel grade S355 and L=26 m). After installation of the SPWs a pre-excavation was carried out to level +10 (2 m depth) followed by installation of the pre-cast concrete piles. In order to minimise mass-displacement and damage to the surroundings, soil was extracted down to level ±0 before installation of each pile. This was carried out by hammering a hollow cylinder with an area corresponding to that of the concrete piles and equipped with a trapper in the end. The pile heads were then hammered to level ca +3 in general. This resulted in mass-displacement below level ±0 and a net outtake of volume above level ca +3. The excavation, including casting of a 0.7 m thick concrete sealing slab, was carried out under water. Steel struts (∅711-14.2 mm) were installed at level +13 in a cc distance of 9 m sequentially with the progress of excavation. Before dewatering, the slab was secured against uplift by the installation of vertical pre-stressed anchors (∅36 mm steel rods) grouted 6 m into bedrock using an early form (Swedish "Lindömetoden") of ODEX-drill system. Final dewatering took place in late August 2003, see Figure B.5. After dewatering, the piles were cut to final levels including exposing the rebars along a length of 700 mm in order to cast the piles into the slab and secure the pile-slab connections.

Figure B.5: *The excavation after final dewatering in August 2003.*

B.2.4 Instrumentation

In addition to the contractors regular monitoring program, the excavation was instrumented and monitored as part of a previous research project at Chalmers University of Technology (Kullingsjö 2007). The instrumentation in section 1/430 is outlined in Figure B.6. In addition to this instrumentation the monitoring included e.g. strut forces and surveying of deformations of the anchored concrete slab, nearby buildings and the sheet pile walls.

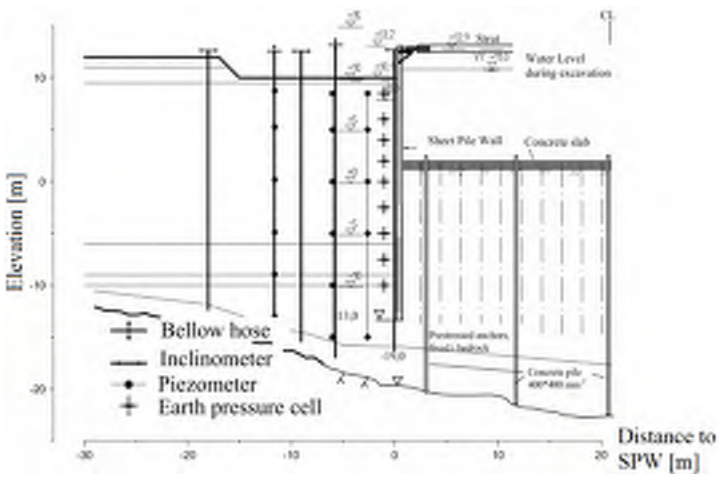

Figure B.6: *Instrumentation in section 1/430 as part of a Chalmers research project at the time of construction. From Kullingsjö (2007).*

B.3 Numerical model

B.3.1 Constitutive soil model

In order to assess the time-dependent response of the construction process including the effect of ongoing background creep settlements, a model that accounts for rate-dependency is needed. Numerical analyses were thus carried out with the Creep-SCLAY1S constitutive soil model, implemented in a 2D finite element software (Plaxis 2D version 2019). The soil model incorporates characteristic soft clay features such as:

- Rate-dependency (visco-plasticity); enables taking into account volumetric and deviatoric creep strains, stress relaxation after pile installation as well as strain rate dependence of shear strength.
- Plastic anisotropy; enables taking into account the inherent plastic anisotropy of natural Gothenburg clay as well as the evolution (increase or loss) of anisotropy due to incorporating a rotational hardening law.
- Destructuration; enables taking into account loss of strength and stiffness due to degradation of bonds in soft sensitive clays.

For model details see for example Wheeler et al. (2003), Leoni et al. (2008), Grimstad, Degago, et al. (2010), Sivasithamparam et al. (2015), Gras et al. (2017), and Gras et al. (2018). One of the main benefits of using a rate-dependent effective stress based model such as Creep-SCLAY1S, is that one unified model parameter set can be used for the predictions of the short- as well as the long-term performance. Further, the model overcomes simplifications of natural clay behaviour which may separately or in combination lead to unsafe design, such as e.g. not accounting for consolidation of negative excess pore pressures after excavation (increasing OCR and thus reduction in shear strength), post-peak strain softening, strain rate dependency of strength and stiffness. However, the Creep-SCLAY1S model does not account for the soil feature of small-strain stiffness, which may be important to consider in modelling and design depending on the type of soil-structure modelling situation at hand.

B.3.2 Model parameters

The model parameters and derived values for the numerical boundary value analysis are presented in Tables B.1 and B.2. Element level simulations of laboratory data are presented in Figure B.8 (CRS oedometer) and Figure B.7 (triaxial tests).

The value of K_0^{nc} was set to 0.42 to be used in the soil model, this is lower than previously measured values ranging from 0.50-0.55 in laboratory tests on Gothenburg clay (Sällfors 1975; Kullingsjö 2007; Olsson 2013). However, it results from the model formulation deriving the value of K_0^{nc} based on the critical state friction angle in compression, M_c. The in-situ K_0 was set to 0.60, this decision was inferred from the equation by Schmidt (1966) using K_0^{nc}=0.525 (average of previous laboratory tests) and ϕ'=30°, which for OCR in the studied section result in K_0 varying between 0.56-0.64.

It should be noted that since the initial analyses of this excavation with the Creep-SCLAY1S model (Tornborg et al. 2019), new incremental load (IL) oedometer tests have been made available by a consultant company (Larsson 2018) for the foundation design of a building partially extending out into the Göta River north of the studied section. IL tests were only performed at samples from depths greater than 55 m, but they are still considered worthwhile for assessing the validity of the creep parameters for the Göta Tunnel case. Based on these tests minor adjustments of model parameters (λ_i^*, ω and μ_i^*) have been made compared to Tornborg et al. (2019). Element level simulations of a IL test is included in Figure B.8. After the initial load increment the predicted strain was offset to the measured strain. Due to κ^* in the element level simulations, being derived from depths (4-25m) at the Göta Tunnel, the simulation overestimate the stiffness in the elastic region when extrapolating to larger depths. The parameter values of the clay layers are presented in Table B.1 and B.2 and the friction material in Table B.3.

Table B.1: Creep-SCLAY1S model parameters for natural Gothenburg clay at Göta Tunnel section 1/430.

Parameter	Definition	Value
λ_i^*	Modified intrinsic compression index	0.085
κ^*	Modified swelling index	0.013
ν	Poisson's ratio	0.20
M_c	Stress ratio at critical state in triaxial compression	1.45
M_e	Stress ratio at critical state in triaxial extension	1.10
ω	Rate of rotational hardening	200
ω_d	Relative rate of rotat. hardening due to deviator strain	1.0
a	Rate of destructuration	8
b	Relative rate of destructuration due to deviator strain	0.5
α_0	Initial anisotropy	0.57
χ_0	Initial amount of bonding	15
μ_i^*	Modified intrinsic creep index	1/550
τ	Reference time	24h

Table B.2: Additional parameters of clay layers at Göta Tunnel section 1/430.

Layer	Level	ρ [t/m^3]	OCR [-]	e_0 [-]	k_x=k_y [m/s]
1	+10 to +3.5	1.53	1.40	2.26	1×10^{-9}
2	+3.5 to +2.5	1.57	1.20	2.10	1×10^{-9}
3	+2.5 to -2.0	1.59	1.10	1.99	1×10^{-9}
4	-2 to -14	1.68	1.20	1.55	5×10^{-10}
5	-14 to -16	1.79	1.50	0.96	1×10^{-10}

Table B.3: Parameters of friction material.

Material set	ρ/ρ' [t/m^3]	E' [MPa]	ν [-]	c' [kPa]	ϕ'[°]	K_0 [-]	R_{inter} [-]
Mohr-Coulomb	2.0/0.8	30	0.3	1	35	1-sinϕ'	0.5

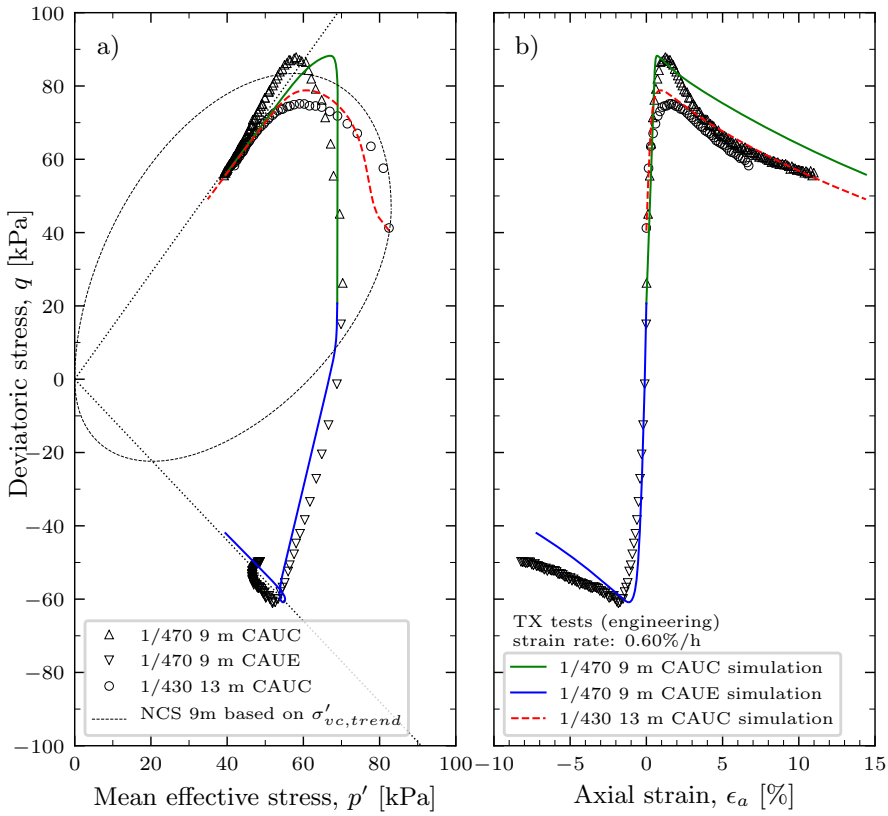

Figure B.7: *Examples of anisotropically consolidated undrained compression (CAUC) and extension (CAUE) tests from sections 1/430 and 1/470 vs. simulations; (a) p'-q-space; (b) plot of ε_a-q. Test 1/430 was consolidated to $\sigma'_{vc(CRS)}/\sigma'_v$=0.94 before shearing whilst in the simulations OCR was set to 1.*

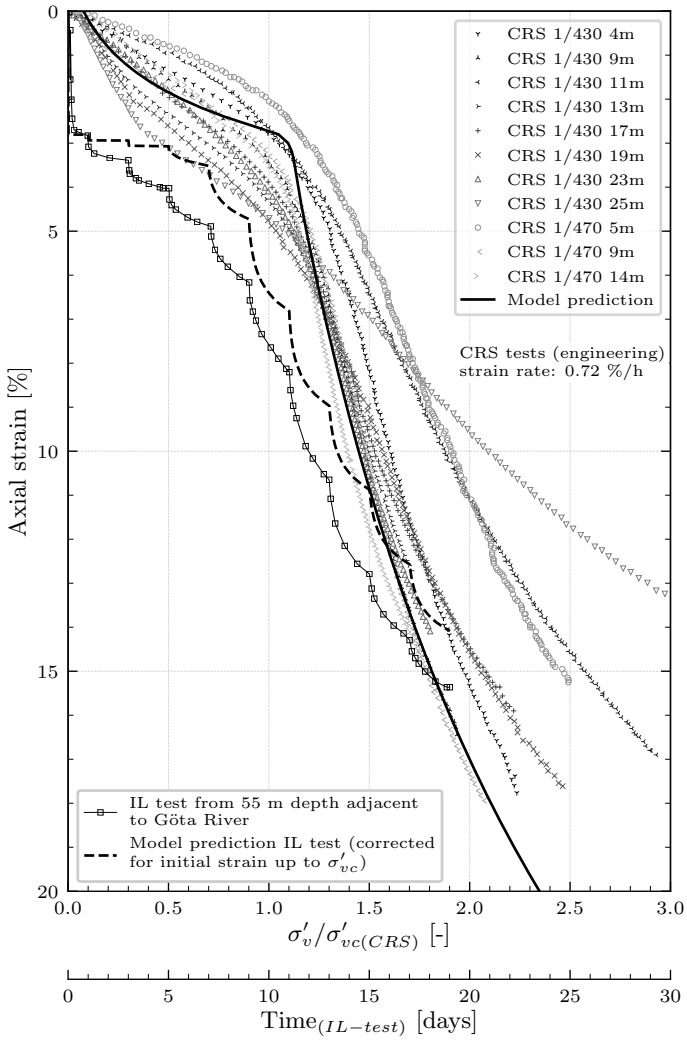

Figure B.8: *Model calibration versus CRS oedometer results as well as calibration against IL test on sample from 55 m depth close to Göta River. IL test simulation corrected for initial strains during first load increment.*

B.3.3 Numerical model geometry, boundary conditions and assumptions

The geometry of the numerical model is given in Figure B.9 and the properties of the structural elements in Table B.4. The construction process was modelled as a time-dependent analyses, with the length of construction activities and intermediate stall-times, see B.5, based on the project logbooks. The effect of nearby buildings (pile foundations) have not been included in this study. Due to the sloping surface of the bedrock, gravity loading was used to generate the initial stresses. The gravity loading was carried out using an adopted value of Poisson's ratio to match the desired in-situ value of K_0. The subsequent stage involved switching to the desired Poisson ratio for the subsequent analyses. The effect of nearby buildings (pile foundations) have not been included in this study. Due to the sloping surface of the bedrock, gravity loading was used to generate the initial stresses. The gravity loading was carried out using an adopted value of Poisson's ratio to match the desired in-situ value of K_0. The subsequent stage involved switching to the desired Poisson ratio for the subsequent analyses.

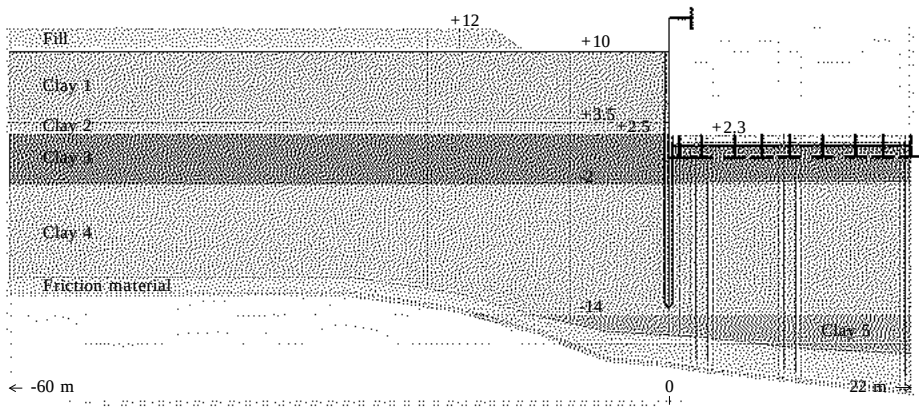

Figure B.9: *Illustration of numerical model geometry including discretised finite element mesh for the boundary value analysis of the excavation (here represented at the stage after dewatering).*

The following assumptions were made with respect to boundary values, structural elements and modelling of installation effects:

- The excavation was modelled as a 2D plane strain problem. The north side of the excavation, containing the instrumentation, was studied and a symmetry line was introduced at the centerline of the tunnel structure. Existing buildings were not included in the model.
- Steady state pore pressures were based on piezometer readings corresponding to level +10, i.e. the top of the clay layer, with an hydrostatic increase towards depth.
- The SPW and vertical model boundaries were assumed impermeable except for the

lower parts of the vertical boundaries, i.e. were friction material is present. The horizontal model boundary below the friction material (i.e. the bedrock interface) was modelled as impermeable in addition to a prescribed line displacement (fixed in vertical and horizontal directions).

- The underwater concrete slab was modelled as a volume with material properties according to Table B.4.
- Installation effects due to the installation of pre-cast concrete piles was modelled with prescribed volumetric strain. As outtake of clay was performed with a hollow cylinder to level ±0, and the pile heads hammered down to level ca +3; negative volumetric strain was modelled above level +3, no volumetric strain between level +3 and +0, and positive volumetric strain below level ±0. The 10 pile rows in the section were installed in pairs of two (Figure B.4). The volumetric strain for each pair of pile rows was calculated and applied as "smeared" over 2 m wide soil clusters. The strain was calculated as (2m× $pile_{ccout-of-plane}$+pile volume)/2m× $pile_{ccout-of-plane}$ corresponding to a volume increase of 8% for the pile row pair in the centerline and 6.5 % for the other pile row pairs. The negative volumetric strain above level +3 was set to 4% and 2% for the centerline and other pile rows respectively. In all cases the strain in the 2D plane strain model was distributed between the horizontal and out-of-plane directions.
- The concrete piles were modelled as embedded beams. During the pre-stressing of the vertical anchors, and building/loading of the main tunnel onto the concrete slab, the concrete piles were connected to the lower model boundary in order to simulate stiff behaviour of the pile toe during compression, i.e. pile toes onto bedrock or stiff friction material. In the other calculation phases the pile toes were free to move.

For studying the impact of installation effects resulting from drilling the vertical anchors, the following approach was applied in the analyses:

- A volumetric strain was introduced based on that the ∅36 mm anchor rods were installed within casing tubes (ca ∅90 mm) during ODEX-drilling to bedrock. The installation of the casing tubes were considered ideal (no mass displacement) and retracting the casing tubes was considered to cause the soil to close the hole around the anchor rod. The volumetric strain was calculated as "smeared" in the soil layers under the slab and over the entire width of the excavation, corresponding to ca -0.1% volumetric strain distributed between the horizontal and out-of-plane directions.
- In addition the material set for the clay layers were set to correspond to intrinsic properties by setting χ_0=0 and OCR=1. The material sets were changed for the clay layers under the entire width of the excavation.
- Installing the casing tubes with a high rate of penetration through clay may resemble that of installing displacement piles, generating excess pore pressures. However, this was not modelled.

Table B.4: Parameter sets for structural elements

Structural element	Material set	Parameter	Value
UW-concrete slab	Mohr-Coloumb	ρ	2.4 t/m^3
	(Drained)	E	30 GPa
		ν	0.20 [-]
		c'	2.0 MPa
		ϕ'	35°
		$k_x = k_y$	1×10^{-9} m/s[1)]
		K_0	1.0 [-]
		R_{inter}	0.2 [-]
		Tension-cut off	Yes (1.6 MPa)
UW-concrete slab	Mohr-Coloumb	ρ, E, ν,	As above
for SPW interface[2)]	(Non-porous)	K_0 and R_{inter}	
		c'	200 kPa
		ϕ'	0°
		Tension-cut off	Yes (0 MPa)
Struts ∅711-14.2mm	Fixed-end-anchor	E	200 GPa
		A	311 cm^2
		cc-distance	9.0 m
Sheet pile walls (AZ36)	Plate	E	200 GPa
		EA	5.2×10^6 kN/m
		EI	173.9×10^3 kN/m^2/m
		w	1.9 kN/m/m
		ν	0.30 [-]
		M_p	1448 kNm/m
		N_p	8552 kN/m
Concrete piles	Emb. beam rows	E	37 GPa
(0.4×0.4 m^2)		$cc_{distance}$	2.4 m [3)]
		$T_{axial,skin}$	$f(0.7c_u)$ kN/m
		$T_{lat,skin}$	1 kN/m

[1)] based on the assumption that the concrete slab was as permeable as the clay due to the number of vertical anchors and concrete piles, e.g. all clay was most likely not rinsed perfectly of the pile surface before casting the slab.
[2)] for the concrete interface connected to the SPW, a separate material set was created with the tension cut-off set to 0 kPa in order to allow for the concrete to separate from the SPW in tension.
[3)] 2.0 m in the pile row in the tunnel centerline.

Table B.5: Calculation phases in the FE-analysis.

Phase	Description	Time [days]
01	Initial stress generation (gravity loading)	-
02	Change to model Poisson's ratio (0.20)	-
03	NIL-step	-
04	Installation of SPW	1 (44)
05	Excavation to +10 (eastern part)	1 (32)
06	Excavation to +10 (within SPW)	4 (38)
07	Pile install. at section 1/430 of pilerows in centerline	8 (-)
08	Pile install. at section 1/430 of pilerows in middle	2 (-)
09	Pile install. at section 1/430 of pilerows closest to SPW	6 (-)
10	Activate embedded beams	1 (37)
11	Fill to +11 within SPW	2 (29)
12	Underwater excavation to level +9	2 (-)
13	Underwater excavation to level +7 and strut installation	2 (-)
14	Underwater excavation to level +6	1 (4)
15	Underwater excavation to final level (+1.6)	6 (79)
16	Casting of 0.7 m thick concrete slab	2 (14)
17	Installation and pre-stressing of vertical anchors	37 (4)
18	Dewatering to level +10	1 (23)
19	Extended unloading excavation (level +10) outside SPW	2 (4)
20	Dewatering to level +9	3 (3)
21	Dewatering to level +6	1 (7)
22	Final dewatering	2 (12)
23	Construction of main tunnel	153 (-)
24	Fill on slab for construction of ramp segment	42 (17)
25	Construction of ramp segment	57 (218)
26	Back-filling to level +12 and cut strut	31 (15)
27	2005 to 2018	5081 (-)
28	2019 settlement rate	365 (-)

All phases except 01-03 are calculated as consolidation analysis. Execution times and stall/consolidation times, given within (), after respective activity are based on the project logbooks.

B.4 Results and discussion

This section present and discuss the model response compared to the measurement data. For clarity, it is divided into three subsections i.e.; background settlement rates, response at three main construction stages and the response over timeseries reaching until ca 2 years after final dewatering of the excavation.

B.4.1 Background settlement rates

The model prediction of long-term settlement rates are outlined in Table B.6 including measured rates as described in detail in Section B.2.1. The current ongoing background settlement rate was predicted to a maximum of 3.5 mm/year in the studied cross section, which is most satisfactory compared to the measurement data.

Table B.6: Measured and predicted settlement rates.

	Prior construction	Present day max
Measured	3-8 mm/yr (Svahn and Liedberg 2001)	2-6 mm/yr (InSAR)
Model prediction	6.2 mm/yr	3.5 mm/yr

B.4.2 Response during main construction stages

Comparisons of model predictions and measurements of horizontal and vertical deformations (Figures B.10 and B.11) as well as horizontal total stresses (Figure B.12) are presented for three stages of the construction process; i.e. after pile installation, underwater excavation and final dewatering. The model predictions capture the trends of deformations well in general, although the absolute values are off by maximum ca 20 mm in the horizontal and ca 15 mm in the vertical direction. This is discussed in detail in the following.

For the stage after pile installation (red markers and lines in Figures B.10 and B.11), the offset is considered to be an effect of the simplified modelling of the pile installation process by prescribing volumetric strain in the horizontal and out-of-plane directions. Furthermore, the pre-extraction of soil down to level ±0 was modelled as a negative volumetric strain (collapse) with an efficiency equivalent to half the volume of the hollow cylinder. Given the results, this too is an oversimplification, as the "smearing" in the 2D-model underestimate the stiffness response of the clay to partially arch around the cavities in the field.

After underwater excavation and final dewatering, the model response in general underestimate the deformations. This is, to some extent, likely due to the wished-in-place modelling of the pre-stressed vertical anchors securing the slab against uplift. The anchors were pre-stressed sequentially under water without post-tensioning, therefore they were most likely not operating under the prescribed pre-stress force at the time for dewatering. Also and more importantly, the installation of the anchors may have disturbed the clay and the friction material. A result of including modelling of installation effects of the anchors is included in Figure B.10 a) and discussed in detail in section B.4.3.

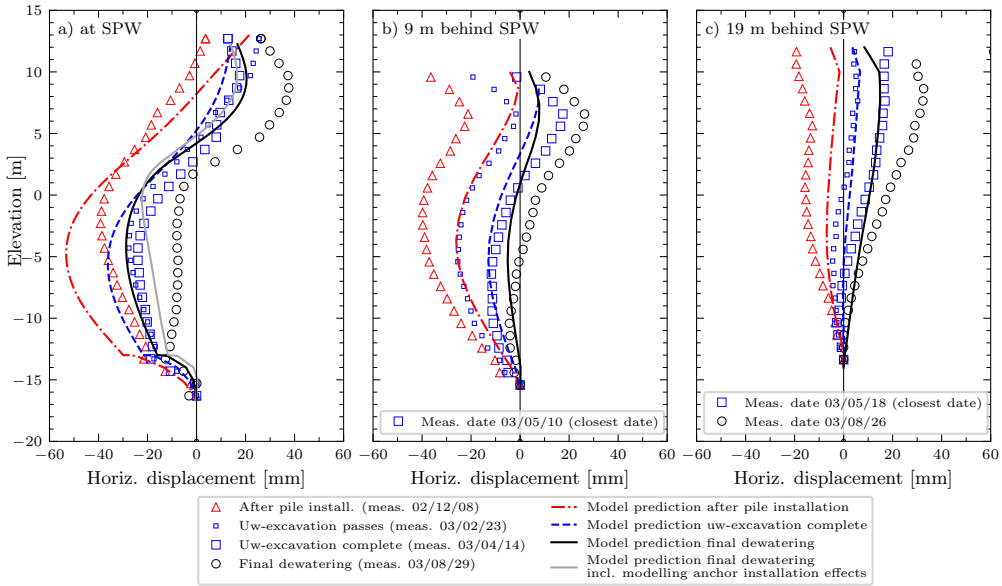

Figure B.10: *Measured versus predicted horizontal displacements at various distances from SPW. Positive values indicate displacement towards excavation.*

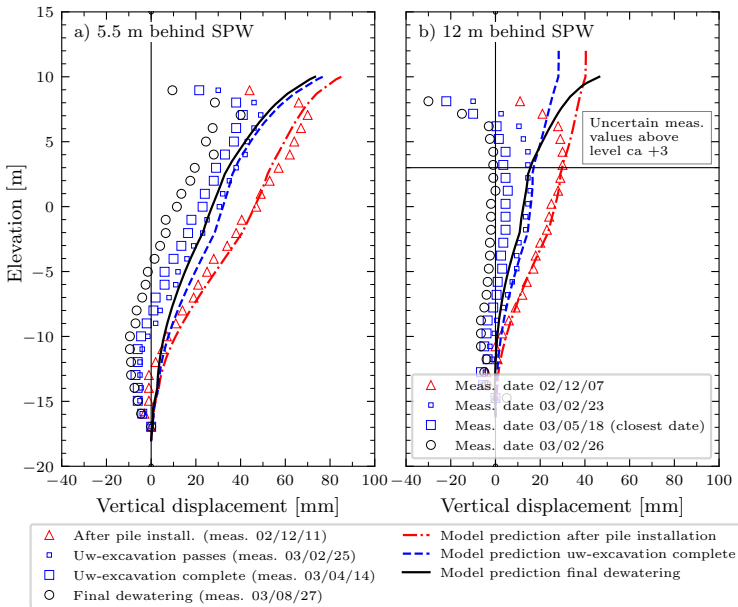

Figure B.11: *Measured versus predicted vertical displacements at various distances behind SPW. Positive values indicate heave.*

Figure B.12 show that the prediction of horizontal total stress at 0.5 m distance behind the SPW (on the retained side) agree well with the measurements. Included in Figure B.12 is also the total overburden pressure before start of construction and at the stage of final dewatering, both obtained from the numerical model. It can be seen that the measured horizontal stress have approached the total vertical overburden. This is most likely caused by an increase in radial stresses due to the pile-installation process and also due to the initial excavation to level +10 which causes K_0 to increase as a result of the increase in OCR. The results of including modelling of installation effects of the anchors under the slab is included in Figure B.12, this results in a slightly but not significantly improved prediction of earth pressures below level ±0.

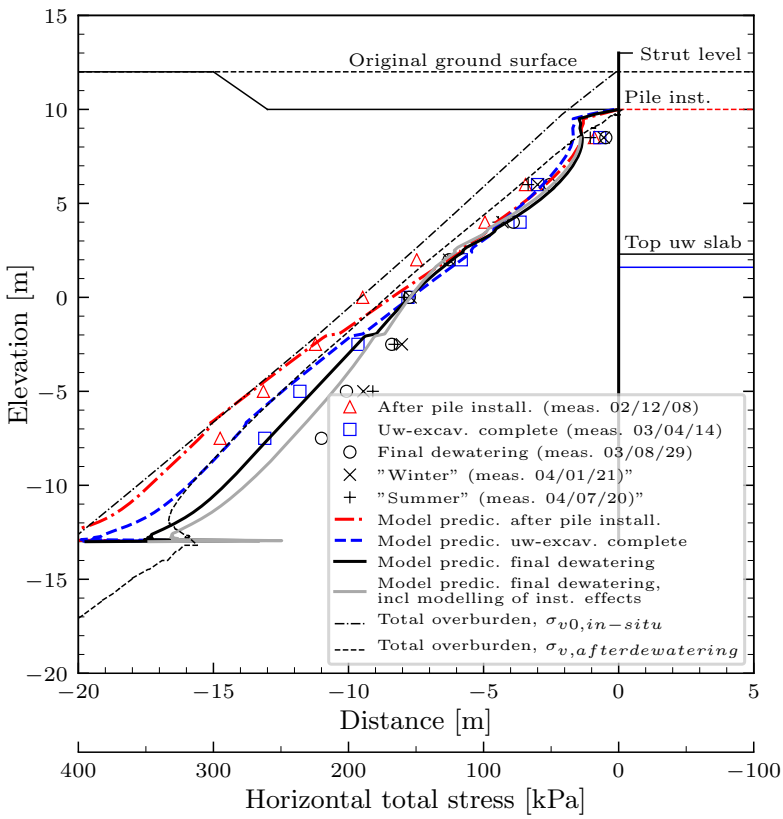

Figure B.12: *Measured and predicted horizontal total stresses 0.5 m behind SPW (retained side).*

B.4.3 Response over time

The following section compares model predictions and time-series of measurement data extending until ca 2 years after final dewatering.

Figure B.13 present measured and predicted pore pressures. The measurements indicate that installation of the sheet pile walls caused notable excess pore pressures which immediately offset the readings close to the wall (SPWs installed mid July 2002). Furthermore, the model response is oversensitive to the initial pre-excavations inside and outside the SPW, and the extreme peaks in pore pressures during pile installation are not captured. This is most likely caused by the simplified modelling of the pile installation process. Nevertheless, the model predictions are in general in very good agreement with the measurements at the time of final dewatering and thereafter.

In Figures B.14 and B.15 the horizontal and vertical deformations are plotted versus time. The main finding from these results is that the horizontal deformations continued to develop towards the excavation in general up to ca 9 months after the final dewatering. Also, the extensometers behind the SPW showed continued settlements. Due to these findings, detailed examinations were made in order to explore plausible explanations such as e.g. vertical upward movement of the anchored concrete slab (Figure B.18), lowering of the pore pressures around the excavation (Figure B.19), shift/horizontal deformation of the entire earth retaining system (Figures B.20 and B.21), as well as revisiting the project log-books and photos. Based on these examinations, our explanation is that the continued deformations most likely were caused, in partial by shift of the entire earth retaining system to the south (10-20 mm horizontal movement), but probably also to a great extent by installation effects arising from the vertical anchors within the studied section and the installation of tie-back anchors and steel core piles in an adjacent part of the tunnel excavation. This finding is based on the fact that the installation of the vertical anchors within the studied section was carried out using top-hammer ODEX drilling which may have caused; disturbance/destructuration of the sensitive clay, increased pore pressures, plastic failure of the clay around the bore holes when pulling the casings (thus resulting in settlements) - this in addition to possible disturbance effects and volume loss (Venturi effect during drilling) in the friction material underneath the clay layer. In total such effects may have resulted e.g. in a void forming under the concrete slab (which was fixated with anchors and concrete piles). The explanation of the severe impact of installation effects from ODEX drilling is supported by the observations in field trials carried out by NGI (Lande and Karlsrud 2015) at a well characterised soft clay site, Onsøy, Norway, similar to the ground conditions at the Göta Tunnel. Additional examples of installation effects due to drilling are given in e.g. Kempfert, H.G. Gebresellassie (1999).

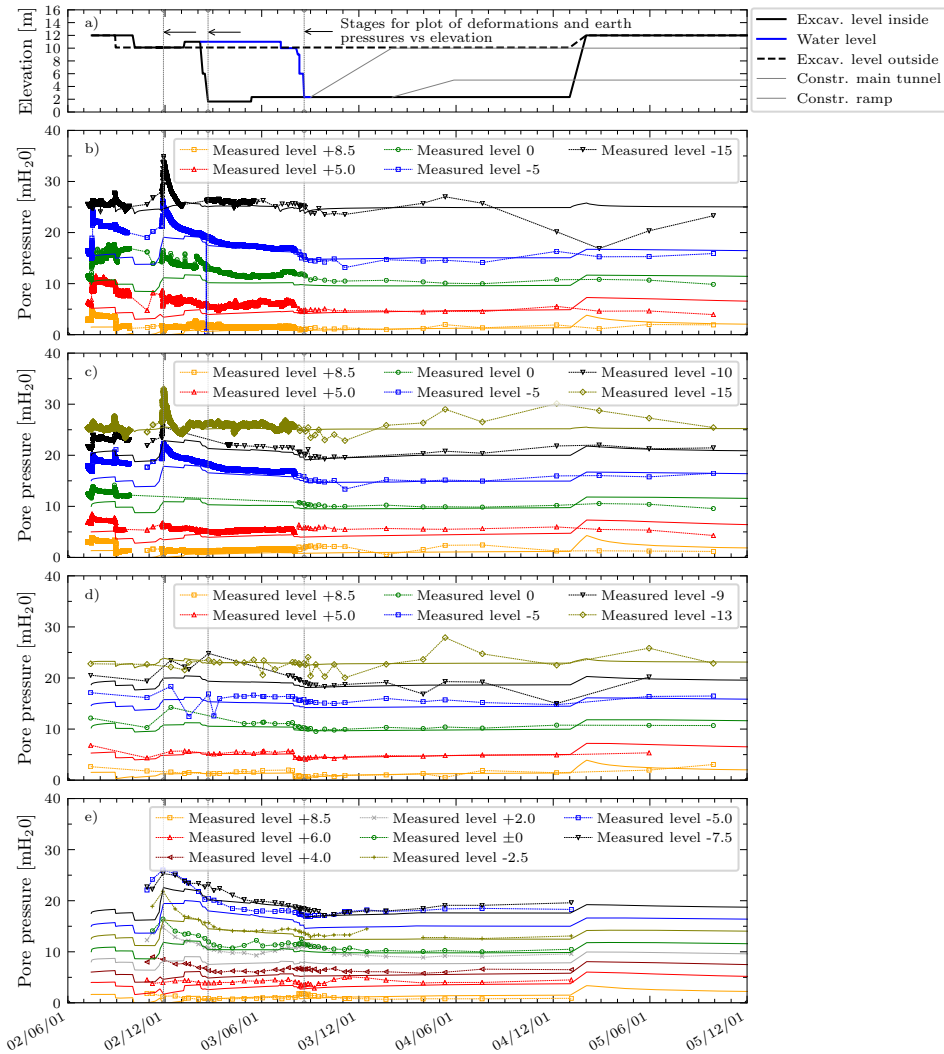

Figure B.13: *Measured and predicted pore pressures a) construction sequence b), c) and d) piezometers located 2.0, 5.5 respectively 10.0 m behind SPW and e) piezometers in earth pressure cells 0.5 m behind SPW. Full lines indicate model predictions.*

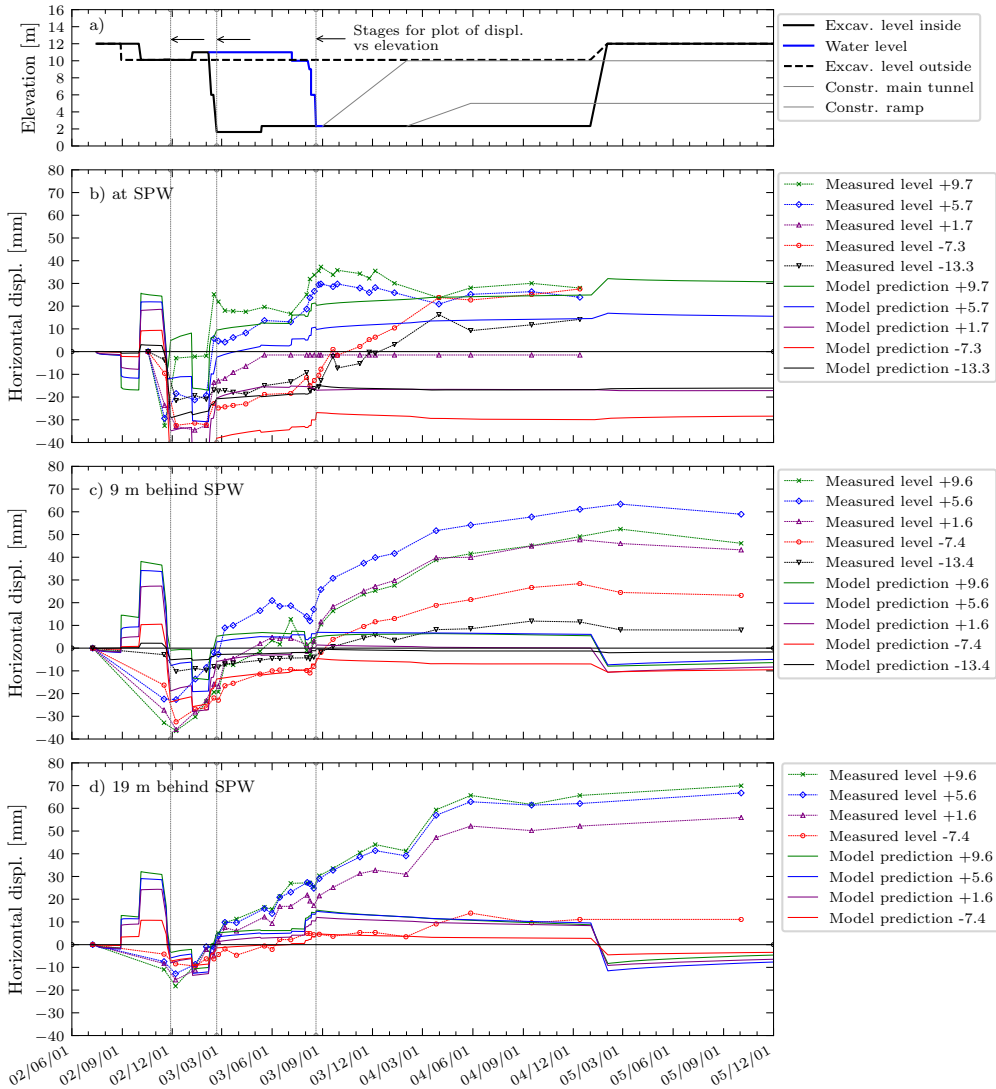

Figure B.14: *Measured and predicted horizontal displacements a) construction sequence b), c) and d) inclinometers at SPW respectively 9 and 19 m behind SPW. Positive values indicate displacement towards excavation.*

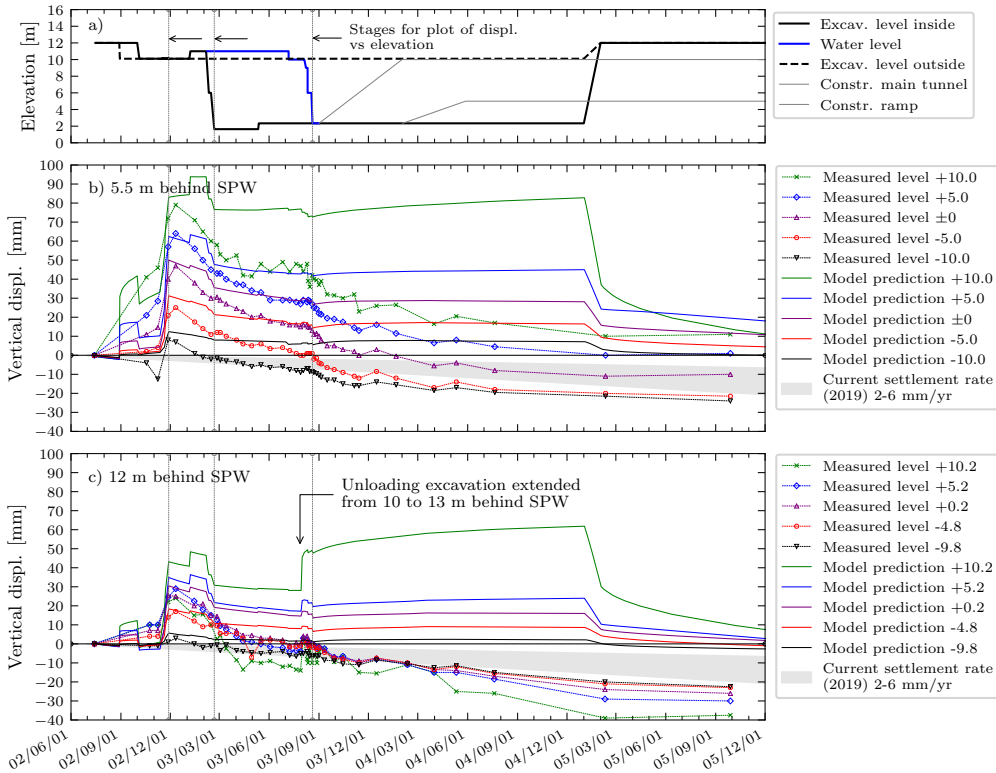

Figure B.15: *Measured and predicted vertical displacements a) construction sequence b) and c) extensometers 5.5 respectively 12 m behind SPW. Positive values indicate heave.*

Figure B.16 present measured and predicted total horizontal stress and strut force including registered air temperature (Swedish Meteorological and Hydrological Institute 2020a). In general the model predictions of total stresses are in good agreement with the measurement data. However, as in the case of the registered pore pressures, the extreme peak values registered during pile installation are not captured in the model. In Figure B.16 c) the response in strut force including results of modelling anchor installation effects is presented. The predicted strut force is in good agreement with the measurement data, yet two things can be noted; 1) the successive installation of struts during underwater excavation was not modelled, hence the model prediction (wished-in-place struts, cc-distance 9 m) underestimate the strut force in the initial stages and 2) the effect of daily and yearly temperature variations on registered strut force is significant, resulting in daily max to min ratios of up to 1.2 after final dewatering and a general decrease in strut force from September to November 2003, followed by a major increase from March to September 2004, almost in parallel with the recorded air temperature increase from winter to summer.

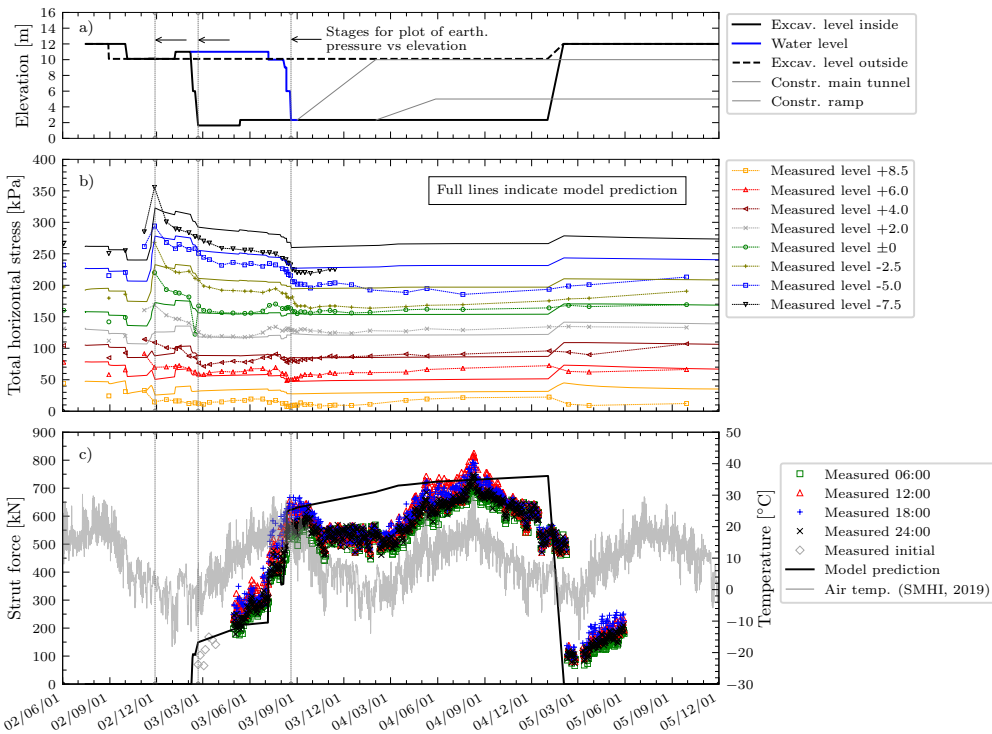

Figure B.16: *Measured and predicted total horizontal stress and strut force a) construction sequence, b) total stresses at 0.5 m distance behind SPW and c) strut force.*

In Figure B.17 the measured and predicted values of K_0 (σ'_h/σ'_v) are presented at 0.5 m distance behind the SPW. In Figure B.17 b) the measured values of K_0 are calculated based on σ'_h ($=\sigma_{h,TPcells}$ - $u_{TPcells}$) and σ'_v ($=\sigma_{v,num.modell}$ - $u_{TPcells}$) with the vertical total stress, $\sigma_{v,num.modell}$, being derived from the numerical model response. The predicted values of K_0 in Figure B.17 b) are calculated based on the numerical model response (i.e. $\sigma'_{h,num.modell}/\sigma'_{v,num.modell}$). In Figure B.17 c) the measured values of a "quasi" K_0 (σ'_h/σ'_{v0}) are calculated based σ'_h ($=\sigma_{h,TPcells}$ - $u_{TPcells}$) and the initial $\sigma'_{v0,num.modell}$ (i.e. a static value, before the start of construction). The predicted values of K_0 in Figure B.17 c) are calculated based on the numerical model response (i.e. $\sigma'_{h,num.modell}/\sigma'_{v0,num.modell}$).

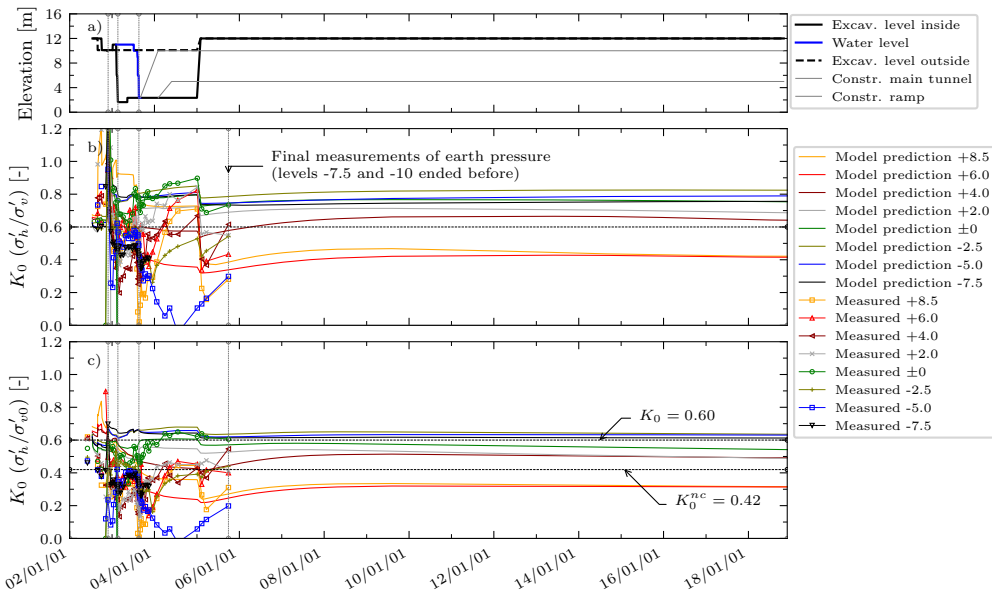

Figure B.17: *Measured and predicted K_0 at location of horizontal earth pressure cells at 0.5 m distance behind SPW a) construction sequence, b) K_0=σ'_h/σ'_v and c) K_0=σ'_h/σ'_{v0}.*

The results of Figure B.17 highlight the variation of K_0 with depth and time. The considerable scatter in the measurement data result from; the impact of construction activities resulting in time-dependent induced stresses and rotation of principal stress, and the fact that the stiffness of the soil and structures varies with depth due to e.g. the support levels of struts and concrete slab. The stiffness of the permanent structure will also effect the earth pressures and long-term K_0 (in the analysis the tunnel was modelled as a linear-elastic block with a stiffness of E=50 MPa). Evaluation of K_0 values are inherently uncertain since it involves; measured horizontal total and pore pressures and calculated total vertical stress - all being associated with some uncertainty. Thus, the predictions are poor compared to measured values, this is in partial also due to the

complexity in modelling excavation problems including the related installation effects and soil-structure interaction. If the horizontal effective stresses have a major impact on the total design pressure against a permanent structure, FE analyses with a rate-dependent soil model still proves a tool to assess the effects of the construction process and system stiffness on the long-term earth pressures. Also, this enables taking into account for example geometry effects and construction activities outside the perimeter of the wall or permanent underground structure including potential increase of earth pressures due to creep deformations.

B.5 Conclusions

This paper has studied a well instrumented section of a part of the Göta Tunnel excavation in Gothenburg. Detailed recollections of project log-books and the extensive measurement data enabled benchmarking of a rate dependent constitutive soil model, Creep-SCLAY1S, against the soil-structure response of an excavation in soft clay. The experiences from the comparison of measurement data and model predictions are summarised in the following in addition to some practical implications:

- Constitutive soil models should account for the necessary features of soft natural clays such as e.g. rate-dependency including creep settlements, anisotropy and destructuration. This enables relevant short and long-term predictions of earth pressures and deformations acting against earth retaining and permanent underground structures. An advantage of advanced rate-dependent effective stress based models is that one unified model parameter set can be used for the predictions of the short-term (construction period, normally the contractors focus) as well as the long-term performance (normally the clients focus). The constitutive model should also ideally account for small-strain stiffness, even though such a feature may not be as important when dealing with very soft clays.
- Continued horizontal and vertical deformations were registered up to ca 9 months after final dewatering. These deformations were likely caused by installation effects resulting from the installation (by means of ODEX-drilling) of vertical anchors within the studied section and the installation of tie-back anchors and steel core piles in an adjacent part of the tunnel excavation. However, the implications of such effects are difficult to predict and model accurately (clay as well as friction material).
- Excavations in urban areas are complex problems to model given the proximity to existing buildings and infrastructure and the level of detail of the construction sequence, causing challenges in estimating the final time-steps beforehand. However, the latter could be overcome if the contractor, the client and the designer work in close collaboration continuously during projects. Further, installation effects should be assessed in the modelling since e.g. initial construction activities such as pile installation may change the in-situ stress state before excavation even has started.
- The measurement of strut force illustrate the effect of daily and yearly temperature variations on registered strut force and thus the importance of considering the current seasonal settings at the time of installing struts intended to be in service

under different climate conditions. Induced thermal loads can comprise of thermal expansion of the steel struts as well as freezing ground behind the sheet pile wall, favourably unlikely in combination.

- The prediction of horizontal total stresses were in general in good agreement with the measurements. The measurements show that pile-installation can have significant impact on the earth pressures. This highlights the importance of considering installation effects in the design of retaining structures as well as permanent underground structures, as the earth pressures may be effected of the adopted construction method and processes. Due to the simultaneous increase in excess pore pressure during pile driving in low permeable soil, the increase in effective stress will be smaller than the total stress increase. However, the excess pore pressures will dissipate with time, thus increases also the horizontal effective stresses - which should be added to the long-term (design/ULS) water pressure to make out the total pressure acting on the structure. In this aspect, pre-augering before pile installation does not only help in reduce the deformations to the surroundings during the pile installation phase, it is also beneficial in reducing the increase in horizontal stresses.
- The measurements of earth pressures as well as the evaluated K_0 over time highlight that long-term earth pressures acting against underground structures are highly dependent on the site specific settings such as; ground conditions including previous loading history, choice of retaining system, geometry of excavation, construction activities and finally the time-dependent response of the soil-structure interaction (soil/structure stiffness ratio) during the short- and long-term. The on-going research will look into generalisation of the impact of such factors. If design of permanent underground structures is based on empirical values of K_0, then it should be noted that K_0 may vary over the depth of the permanent structure. If the horizontal effective stresses have a major impact on the total design pressure (σ'_h+u) against a permanent structure, FE analyses with a rate-dependent soil model proves a tool to assess the effects of the construction process and system stiffness on the long-term earth pressures. If so, sensitivity analyses should include to vary for example the model value of K_0^{nc}.

Finally, the paper has presented the experiences from comparing the model response of a advanced constitutive soil model to the field scale response of soil-structure interaction of an well instrumented excavation. The ongoing research project also involves measurements of the long-term response under a permanent structure as well as generalisation of the soil-structure response of underground structures in soft clay. This will provide additional valuable insights on the development of the stress states and earth pressures acting against underground structures as well as highlight (quantify) the factors influencing long-term earth pressures.

B.6 Additional figures, to be appended to Göta Tunnel paper

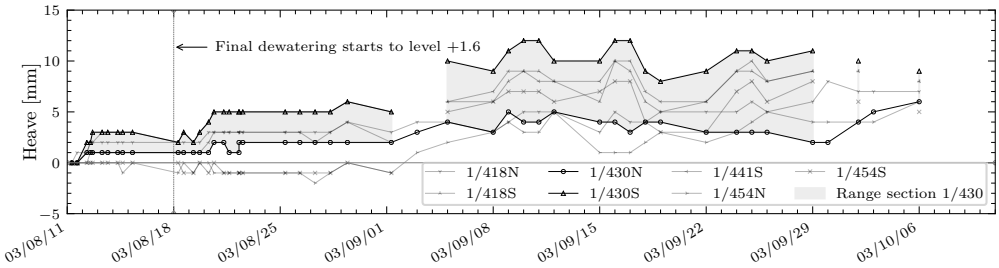

Figure B.18: *Vertical displacement of the anchored concrete slab.*

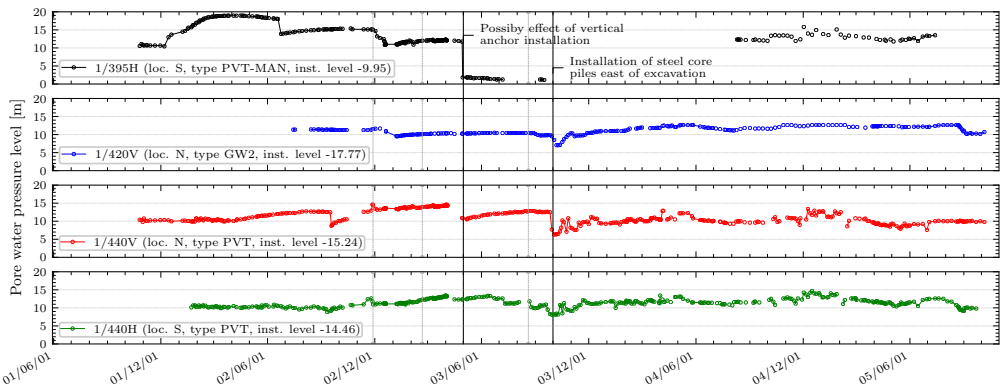

Figure B.19: *Monitoring of pore pressure in bottom of clay layer (PVT) and friction material (GW) adjacent to studied section 1/430. No significant effect in the measurements (section 1/420) closest to the studied section. Further, no indication of lowering of pore pressures indicated in piezometer readings presented Figure B.13.*

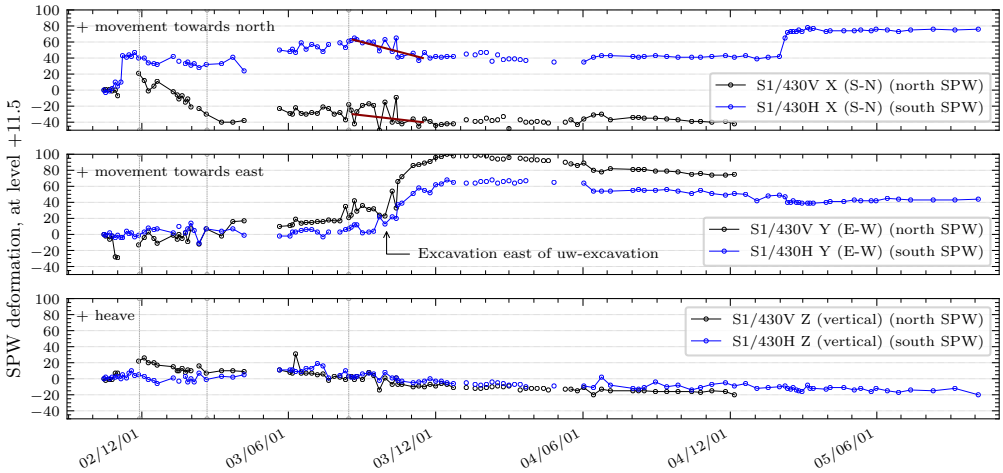

Figure B.20: *Surveying of displacements at level +11.5 on the retaining walls (north and south SPWs). Possible trend in SPW-system shifting 10-20 mm to the south 3 months after final dewatering is indicated by red marker lines.*

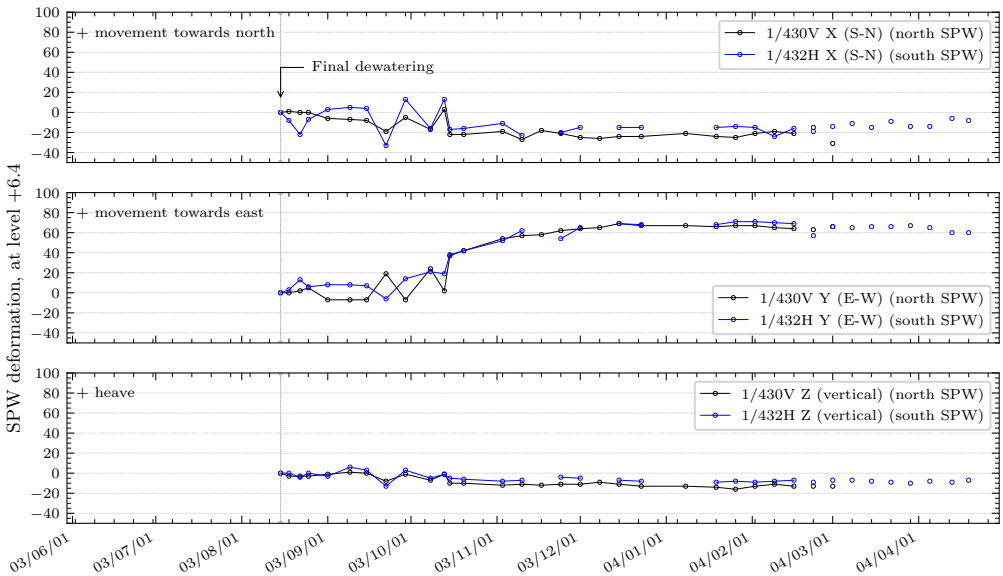

Figure B.21: *Surveying of displacements at level +6.4 on the retaining walls (north and south SPWs).*

C Appendix - Instrumented site additional information

This appendix includes additional data and measurement results from the Hisings Bridge site.

C.1 Site characterisation

Figure C.1 show a satellite photo including the location of the excavation before start of the construction works in September 2018.

Figure C.1: *Outline of the site before start of construction works.*

Previous soil investigation points in the area are presented in Figure C.2, selected points of interest for this study are highlighted with red circles. The excavation for the West Link tunnel is outlined north of the instrumented excavation.

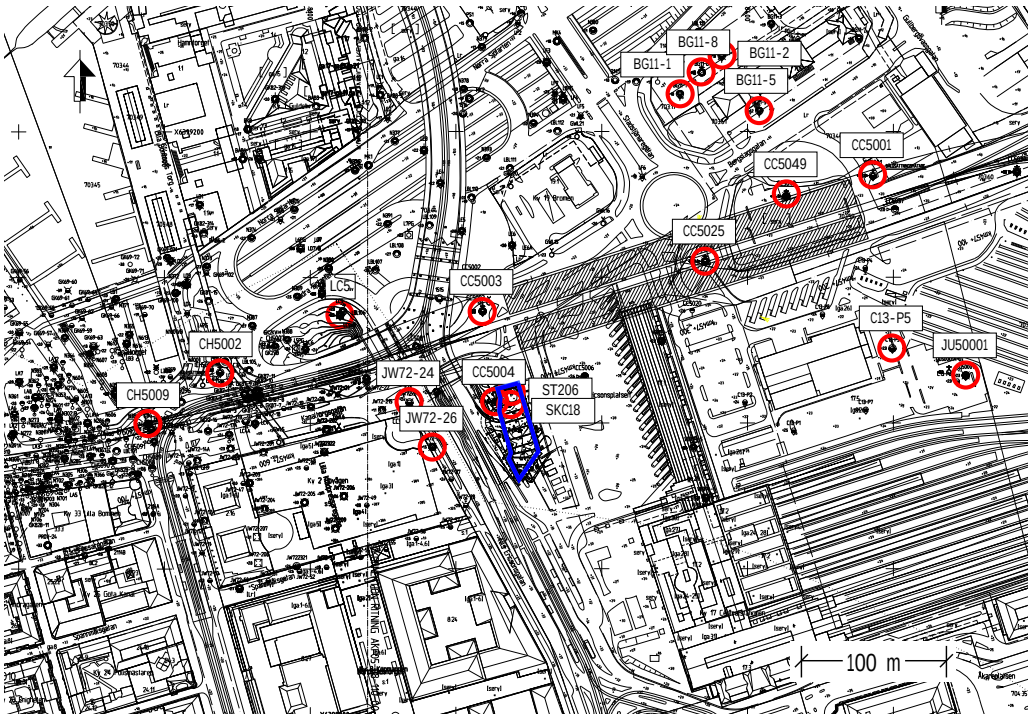

Figure C.2: *Site plan including previous soil investigation points. Selected points of interest for this study are highlighted with red circles. The perimeter of the instrumented excavation is highlighted in blue.*

C.1.1 Pore pressure

Collected data of measurements of pore water pressures in the clay layer are presented in Figure C.3, indicating a pressure level corresponding to approximately +1 with a hydrostatic increase towards depth. As a reference the mean water level of the Göta River is +0.15 (system RH2000) at the location of the Göta River bridge.

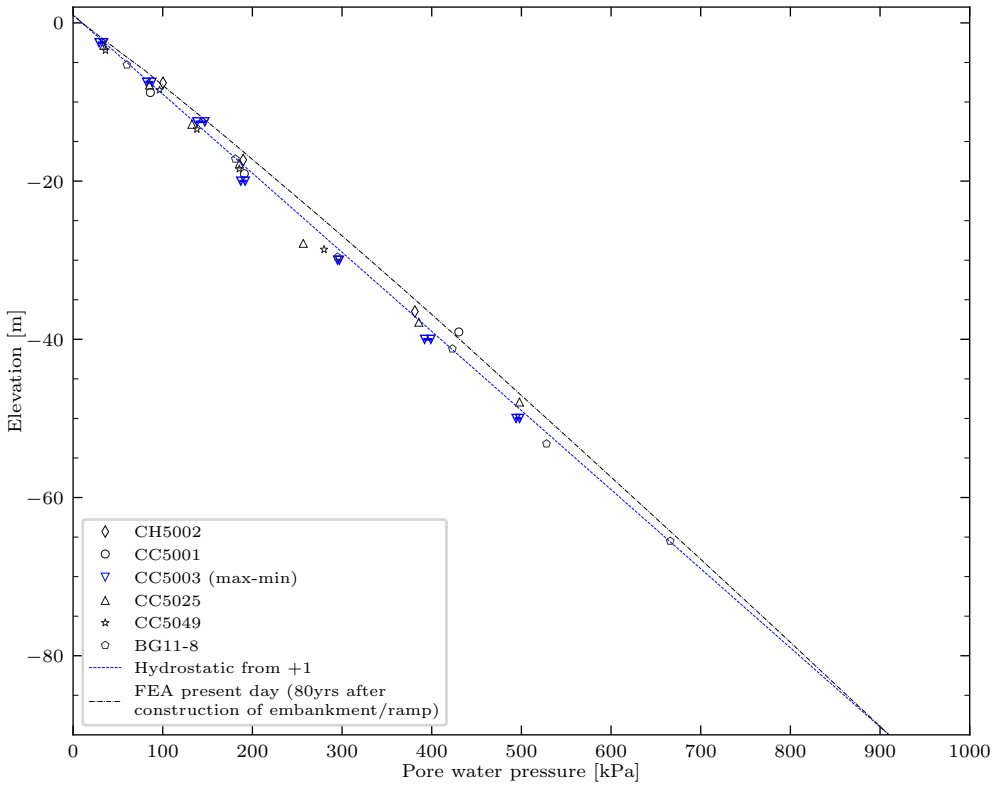

Figure C.3: *Compilation of measurements of pore water pressure in the clay layer. The line for the FE analyses is extracted from initial FE analyses at the end of a stage covering 80 years consolidation after construction of the existing embankment/ramp west of the excavation.*

The rate of on-going settlements in the area before the start of the construction works is presented in Figure C.4 based on InSAR satellite imaging (courtesy of Swedish Transport Administration).

The outline of the old shoreline, defence lines, canals and the locomotive workshop is presented in Figure C.5 where the location of the studied site has been indicated.

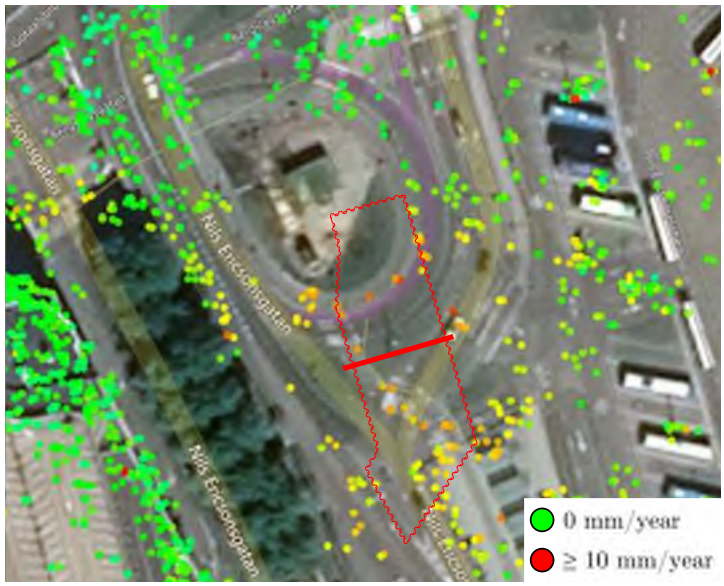

Figure C.4: *Rate of on-going settlement in the area. Courtesy of Trafikverket. The sheet pile walls and the instrumented section are outlined in red.*

Figure C.5: *Historical maps of Gothenburg City a) 1790 b) 1820 c) 1860 and d) 1921. The approximate location of the studied excavation is highlighted with black dashed circles.*

The location and details of the embankment west of excavation is presented in Figure C.6. The embankment is partially founded on 5" wooden piles 15-17 m long.

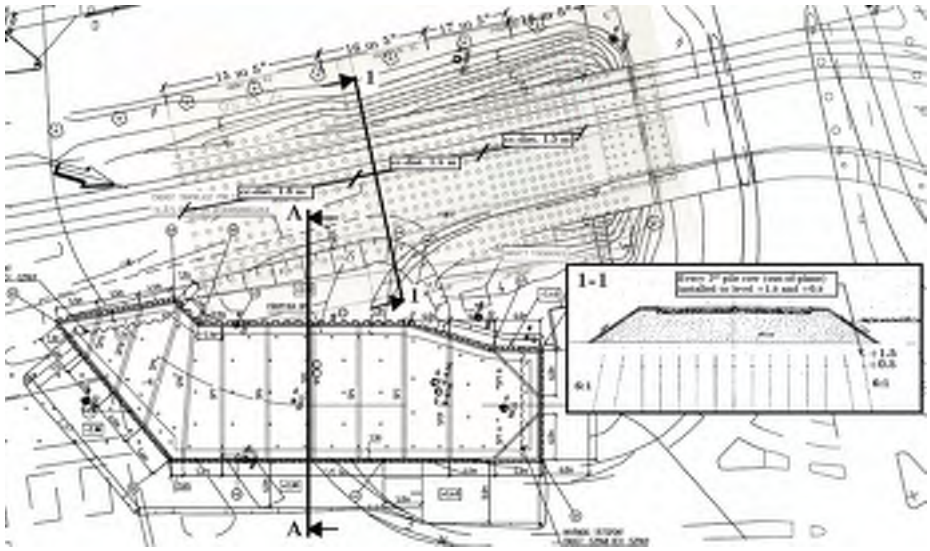

Figure C.6: *Plan of excavation and permanent structure in relation to wooden piles under the existing bridge ramp/embankment. For section A-A, refer to Fig. 4.4.*

C.1.2 Individual plots of drained triaxial tests

This section presents individual plots of the performed drained triaxial tests. These triaxial tests were compiled and presented together with the undrained tests in Figures 4.17 and 4.18.

Plot of drained "active" tests by decrease of radial stress: As outlined in the report (section 4.3.3.2), two drained "active" triaxial tests were carried by means of a constant decrease of the radial total stress (-0.03 kPa/min) under a constant vertical total stress. These tests were carried out in order to more accurately resemble the imposed idealized loading and volumetric conditions on the retained side of excavations and presented in Figures C.7 to C.10. Since the axial strain rate varies during such a test (in order to keep up with deformations as the radial stress decreases) the recorded strain rates are presented in Figures C.8 and C.10.

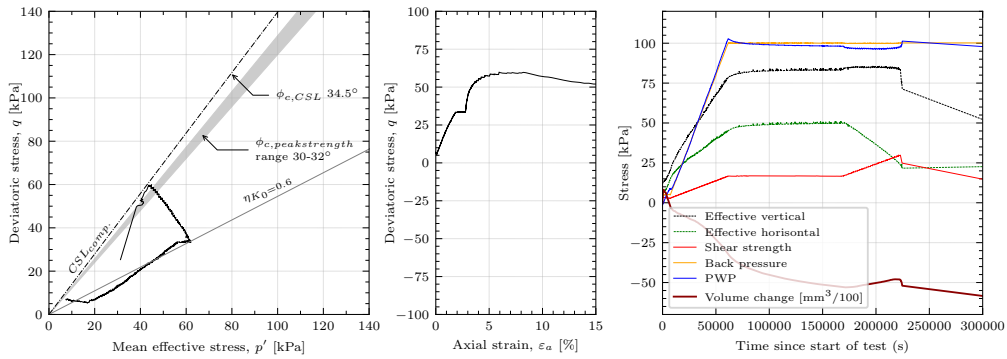

Figure C.7: *Triaxial CAD "active" test on sample from level -6.4 performed as constant decrease of radial total stress (-0.03 kPa/min) under constant vertical total stress.*

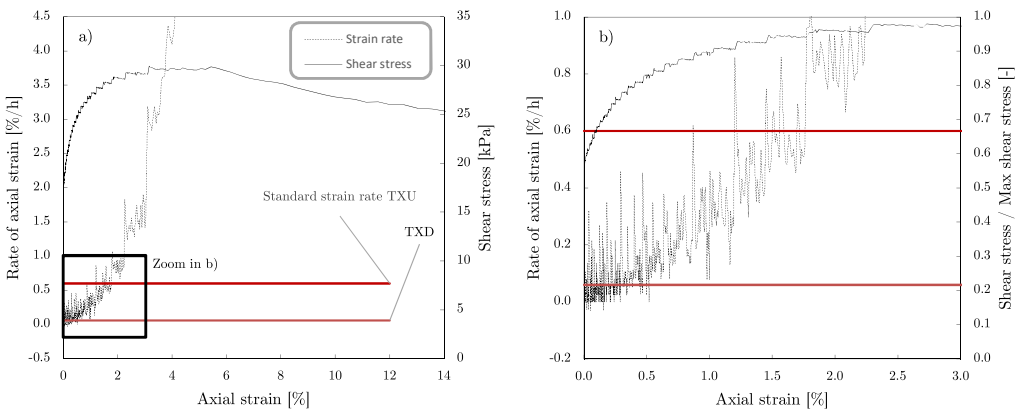

Figure C.8: *Strain rate and shear stress in triaxial CAD "active" test on sample from level -6.4.*

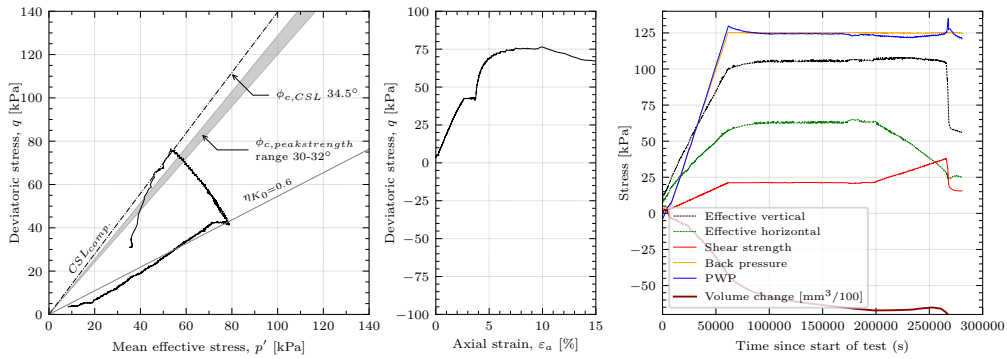

Figure C.9: *Triaxial CAD "active" test on sample from level -11.2 performed as constant decrease of radial total stress (-0.03 kPa/min) under constant vertical total stress.*

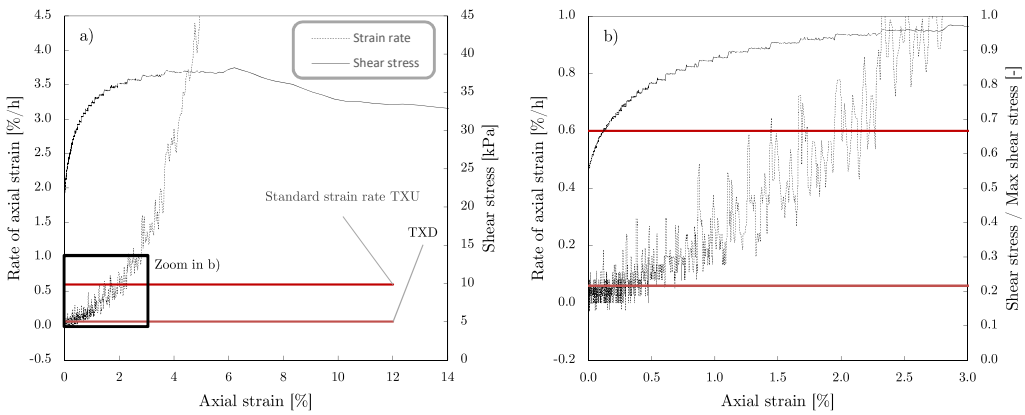

Figure C.10: *Strain rate and shear stress in triaxial CAD "active" test on sample from level -11.2.*

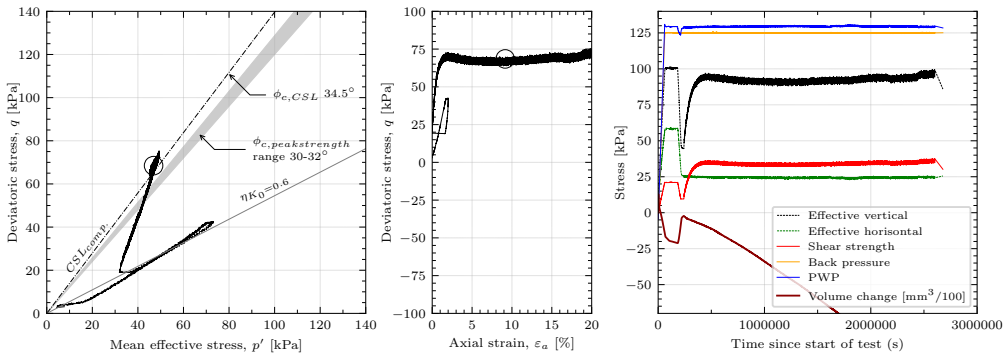

Figure C.11: *Conventional triaxial CADC test (axial deformation 0.001 mm/min corresponding to (engineering) strain rate 0.06 %/h for H=100 mm sample) on sample from level -11.4. After consolidation stage, test unloaded to higher OCR (along K_0=0.6 line) in order to investigate if the test would "hit" the same point of the CSL as the CADC test performed on the sample from level -11.4. (Fig. C.9).*

Plot of drained test with unload-reload cycles: A drained test with unload-reload cycle was performed on a sample from level -15.3, se Figure C.12. A threshold level for change in soil response during extension is distinguishable (for example in volume change) at a vertical effective stress of level corresponding to $0.25\sigma'_{vc,trend}$=0.25*171=43 kPa. Such a threshold level was discussed in the report section 2.2.6 and by Larsson (1977) set to approximately $0.4\sigma'_{vc,trend}$.

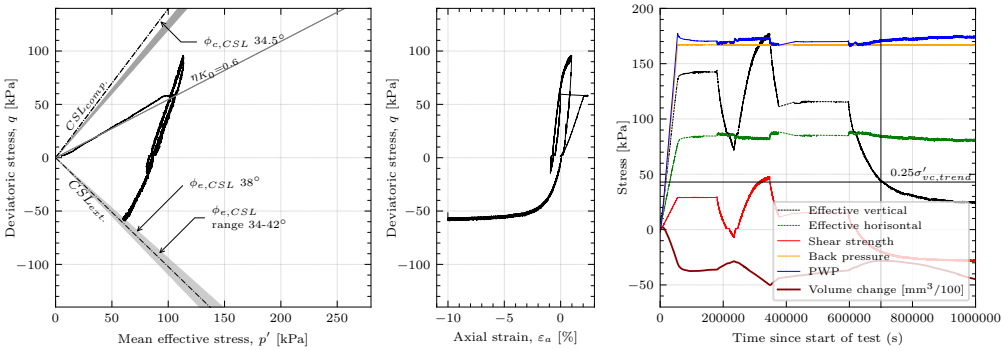

Figure C.12: *Triaxial CAD test on sample from level -15.3 with unload-reload loop followed by unloading to failure in extension.*

C.1.3 Plots of vertical strain versus time for IL tests on remoulded clay samples

This section presents data from IL tests on remoulded clay samples for the evaluation of modified intrinsic creep index, μ_i^*. The stress-strain response for these tests is presented in the report Figure 4.12.

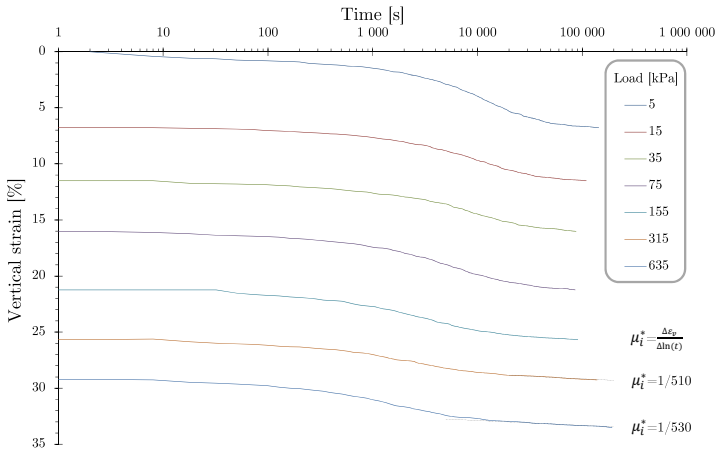

Figure C.13: *IL test on remoulded clay sample from level -4.2.*

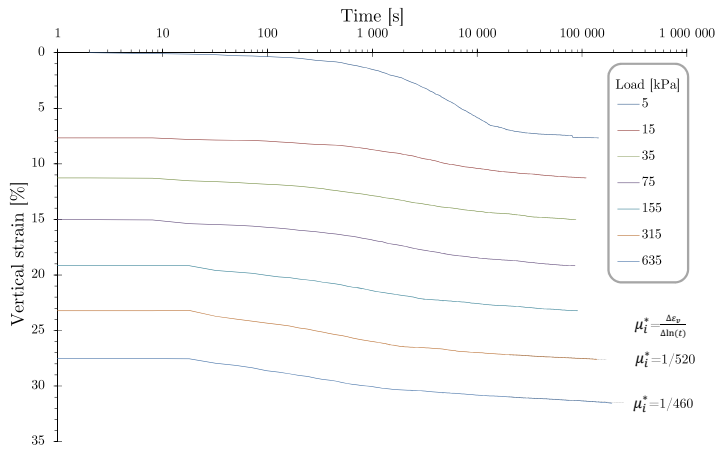

Figure C.14: *IL test on remoulded clay sample from level -7.4.*

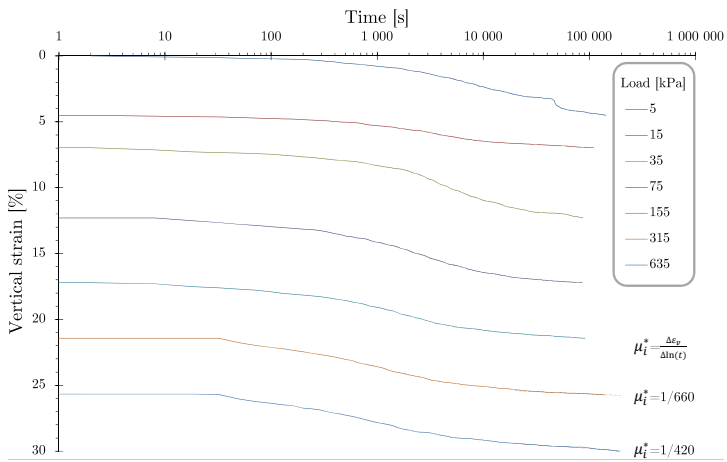

Figure C.15: *IL test on remoulded clay sample from level -17.2.*

C.2 Calibration factors for VW sensors

This section of the appendix present the calibration and correction factors for the VW sensors as well as the results of the verification of the sensor calibration factors. The methodology for this verification is described in the report, section 4.4.6.

C.2.1 Calibration factors and equations supplied by manufacturer

Interpretation of total earth pressure and piezometer readings were made using a linear equation including correction for change in temperature and barometric pressure. According to the manufacturer the equation is:

$$Pressure(kPa) = CF(R_0 - R_c) + (B_0 - B_c) - CFT_{wv}(T_0 - T_c) \quad \text{(C.1)}$$

Regarding the total earth pressure cells; as temperature also affects the pressure due to thermal expansion of the hydraulic fluid inside the cell (e.g. Daigle and Zhao 2004; Huntley and Valsangkar 2016), the equation that has been used to evaluate total pressures reads:

$$Pressure(kPa) = CF(R_0 - R_c) + (B_0 - B_c) - CFT_{wv}(T_0 - T_c) + CFT_{cell}(T_0 - T_c) \quad \text{(C.2)}$$

where subscripts 0 and c refers to initial and current readings. The initial/reference site zero readings were recorded just before installation of each cell. CF is a (linear) calibration factor for converting readings, R (raw units in $Hz^2/1000$), to pressure. B and T are barometric pressure (kPa) and T temperature readings (°C). CFT_{vw} is a linear temperature correction factor, the subscript vw has been added here to clarify it applies only to the VW transducer itself. Both CF and CFT_{vw} are specified by the manufacturer and listed in Table C.1. The CFT_{vw} for the total earth pressure cells (including the 3rd part of eq C.1) were supplied after communication with the manufacturer in 2020 (not specified on the original calibration protocols).

The calibration, CF, and correction factor, CFT_{vw}, supplied by the manufacturer are given in Table C.1. The CFT_{vw} in the case of the total earth pressure cells only applies to the VW transducer itself and does not account for temperature correction with respect to thermal expansion of the cell body including the hydraulic fluid. This has been described in the report, section 4.4.6.1. Therefore the temperature correction factor applying to hydraulic fluid in the cell is introduced, CFT_{cell} in eq. C.2. CFT_{cell} can be estimated based on Sellers 2000 (eq. 4.4), by laboratory calibration or field data from periods where the load is assumed constant but temperature varies. The latter approach was recommended by e.g. Tesarik et al. (n.d.) since it reflects the temperature dependence of the entire cell in field boundary conditions. Sellers eq. 4.4 was however used to provide an indication of the magnitude of CFT_{cell} as installed in the clay at the site. CFT_{cell} was estimated to 0.2-0.3 kPa/°C by taking a=1.5, E=20 to 30 MPa and from communication with the cell manufacturer; K=500×10^{-6}/°C for the hydraulic fluid, D=1.52 mm and R=114 mm.

Table C.1: Manufacturers VW sensor calibration and correction factors.

Sensor type and ID	Location in field	CF [kPa/raw unit]	CFT_{vw}^{1} kPa/°C
Piezometers			
57760	West of CL	0.09602	0.3046
57762	Centremost	0.09364	0.3313
57763	East of CL	0.09167	0.3273
57765	Ref. at logger	0.09319	0.4259
Total earth pressure cells			
3765	West of CL, vertical stress	0.17888	-0.3231
3766	West of CL, horiz. stress	0.18270	-0.3051
3769	Centremost, vertical stress	0.18628	-0.3135
3770	Centremost, horiz. stress	0.18193	-0.3059
3771	East of CL, vertical stress	0.18089	-0.3362
3772	East of CL, horiz. stress	0.18848	-0.3220

[1)] Correction factor with respect to change in temperature which only account for temperature correction of the WV transducer itself. In the case of the total earth pressure cells it does not account for temperature correction with respect to the cell body including the hydraulic fluid. The different sign convention for the piezometers and total pressure cell VW transducers stems from (personal communication with manufaturer): *The sensors are manufactured in batches of 50, with each batch resulting in a slightly different finished product (in terms of material properties) due to the multiple welding and heat treatment processes.*

However, the period from casting of the working platform over the instruments up until the casting of the concrete slab was used to assess the cells total sensitivity to change in temperature with the actual boundary conditions in the field. For the TP cells measuring the vertical stress the temperatures used for correction are assumed to be the same in the location of the thermistor (in the VW housing) as in the hydraulic cell fluid since the cells were laid out flat on the ground surface. For the vertical cells; the temperatures in the VW housing is recorded by the thermistor, however the body of hydraulic cell is located approximately 0.7 m below and the temperatures for correcting with respect to hydraulic cell fluid were therefore based on the piezometer thermistors.

The adopted CFT values are summarized in Table C.2 and have been used for temperature correction throughout the report. Future readings may however provide additional information for improved CFT factors to apply for back-correction of measurement data.

Table C.2: Adopted temperature correction factors for total pressure cells.

Sensor type and ID	Location in field	CFT_{vw} kPa/°C	CFT_{cell} kPa/°C
3765	West of CL, vertical stress	-0.3231	0.28[1)]
3766	West of CL, horiz. stress	-0.3051	0.10[2)]
3769	Centremost, vertical stress	-0.3135	0.29[1)]
3770	Centremost, horiz. stress	-0.3059	0.10[2)]
3771	East of CL, vertical stress	-0.3362	0.26[1)]
3772	East of CL, horiz. stress	-0.3220	0.10[2)]

[1)] Based on the evaluation of temperature sensitivity from field measurements chosen so that the total temperature correction factor in eq. C.2 equals $+0.6(T_0\text{-}T_c)$

[2)] T_0 and T_c based on piezometer thermistors. Slightly lower estimation of CFT_{cell} due to centre level of hydraulic cell bodies located even deeper into the clay than the piezometers (temperature variations and the need for temperature correction decreasing with depth).

C.2.2 Verification of piezometer calibration factors

A photo of the customized pressure cell used for verification of the calibration factors, CFs in Table C.1, for the vibrating wire piezometers is given in Figure C.16. The applied pressures were registered with a DPI800P instrument (manufactured by General electric) with an accuracy of ±0.01 % FS (i.e. ±0.07 kPa for range 0-700 kPa). Verification of each piezometer was made under a condition of constant temperature (during the set of verifications the temperature in the water tank ranged from 18.5 to 18.9°C).

The results of the verifications are presented in Figure C.17 as calculated versus applied pressure. Based on this verification, the CF calibration factors supplied from the manufacturer were kept unadjusted for the field measurements. Additionally the CFT temperature correction factors supplied from the manufacturer were used in order to correct for temperature effect on the WV-transducers.

Figure C.16: *Pressure cell for verification of calibration factors for VW piezometer sensors.*

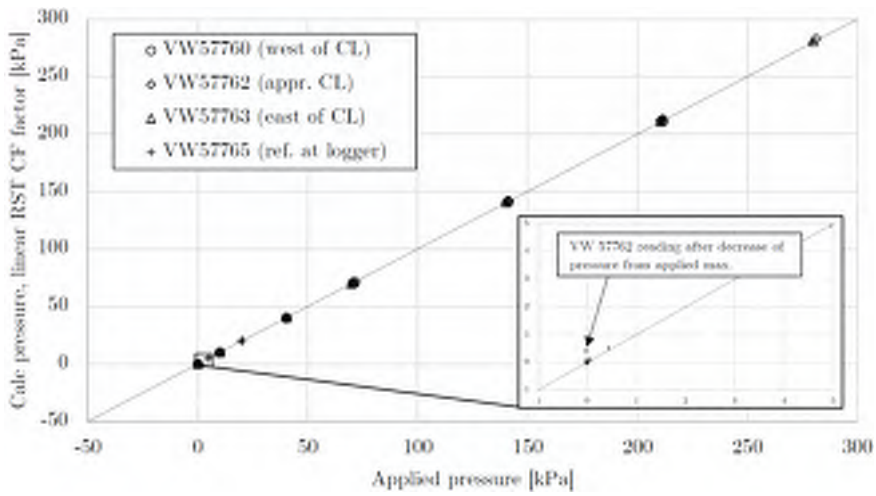

Figure C.17: *Results of verification of calibration factors for VW piezometers. Plot of pore pressure calculated by piezometer readings and RSTs supplied calibration factors versus applied pressure measured with the DPI1800P instrument.*

C.2.3 Verification of total earth pressure cells calibration factors

A photo of the test cell used for verification of the sensor calibration factors, CFs in Table C.1, for the vibrating wire total earth pressure cells is given in Figure C.18. The applied pressures were, as in the case of the VW piezometers, registered with a DPI800P instrument and the verifications were made under conditions of constant temperature.

Figure C.18: *Pressure cell for verification of calibration factors for VW total earth pressure sensors. The cell was assembled using clamps, since it had to be disassembled and reassembled for mounting of each of the total pressure cells (10 in total; 6 installed under the slab plus 4 additional which were decided to not install).*

The results of the verifications are presented in Figure C.19 as calculated versus applied pressure. During pressurizing of the cell, air leakage occurred trough the fibers of the wooden plates at the top of the cell (this was observed by spraying the cell with soap water). This caused differences in the readings of calculated versus applied pressure since the pressure was applied in the top of the test cell and the total earth pressure cells located in the bottom. The observed air leakage was most prominent for pressures above ca 70 kPa which can also be seen in the plot of the verification results. For lower pressures, in the excepted field range, the test cell worked satisfactory and the calculated and applied pressures were in good agreement. Based on the verifications, the CF calibration factors supplied from the manufacturer were kept unadjusted for the field measurements. Additionally the CFT temperature correction factors supplied from the manufacturer were used in order to correct for temperature effect on the WV-transducers.

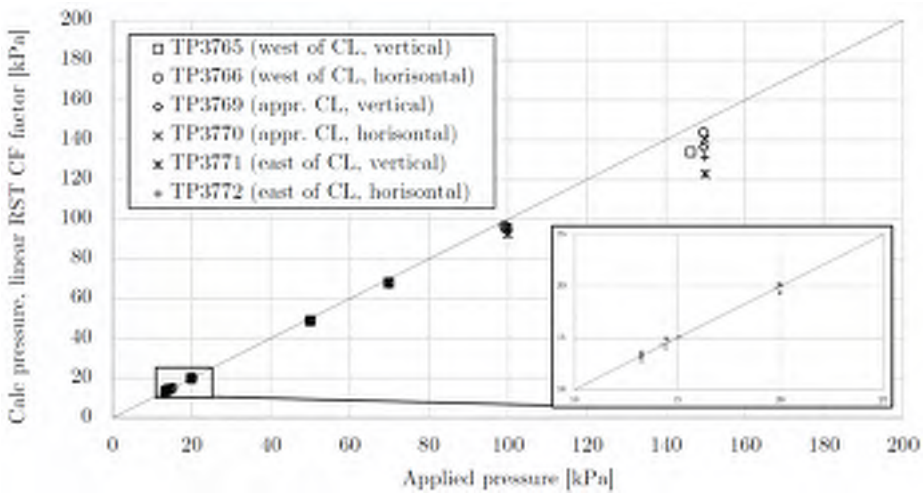

Figure C.19: *Results of verification of calibration factors for VW total earth pressure cells. Plot of pressures calculated by total earth pressure readings and RSTs supplied calibration factors versus applied pressure measured with the DPI1800P instrument. Differences for pressures above ca 70 kPa caused by leakage in test cell.*

C.2.4 Verification of thermistors

The verification of the thermistors in the VW piezometers and earth pressure cells are presented in Table C.3.

Table C.3: Verification of thermistors in VW sensors.

Location for verification and sensor ID	Location in field	Temperature in thermistor °C]	Temperature in calibration thermometer[1)] [°C]	Diff. [°C]
Piezometers				
Water tank				
VW57760	West of CL	17.04	17.0	0.04
VW57762	Centremost	17.03	17.0	0.03
VW57763	East of CL	17.04	17.0	0.04
VW57765	Ref. at logger	17.10	17.0	0.10
Climate room[2)]				
VW57760	West of CL	9.60	9.65	-0.05
VW57762	Centremost	9.47	9.65	-0.18
VW57763	East of CL	9.42	9.65	-0.23
VW57765	Ref. at logger	9.55	9.65	-0.10
TP-cells				
Room temp.				
3765	West of CL, vertical stress	22.1	21.8	0.3
3766	West of CL, horiz. stress	22.0	22.0	0.0
3769	Centremost, vertical stress	21.7	21.4	0.3
3770	Centremost, horiz. stress	21.5	21.8	-0.3
3771	East of CL, vertical stress	21.6	21.8	-0.2
3772	East of CL, horiz. stress	21.8	21.7	0.1

[1)] Average reading of two calibration thermometers.
[2)] Not in operation for geotechnical testing at the time of verification of thermistors due to upcoming move of the laboratory.

C.3 Detailed layout of VW sensors installed under the permanent structure

C.3.1 Total earth pressure cells and piezometers

A detailed layout and cross section of the vibrating wire (VW) sensors (total earth pressure cells and piezometers) installed in the clay under the permanent concrete structure is given in Figure C.20. This layout was adopted for installation at three locations in the instrumented section (overview of instrumentation presented in Figure 4.22).

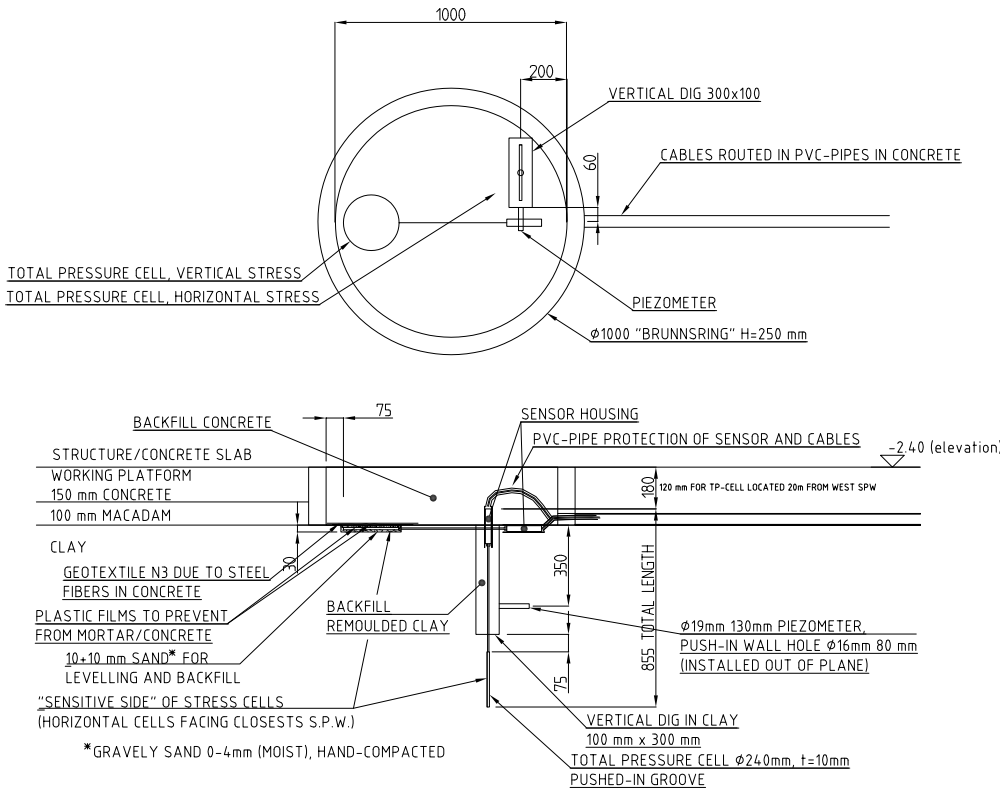

Figure C.20: *Detailed layout and cross section of the total earth pressure cells and piezometers installed in the clay under the permanent structure. Layout adopted at three locations in the instrumented cross section.*

C.3.2 Extensometer

A cross section of the VW extensometer installed in the clay under the permanent concrete structure is given in Figure C.21. The location of the extensometer is presented in Figure 4.22).

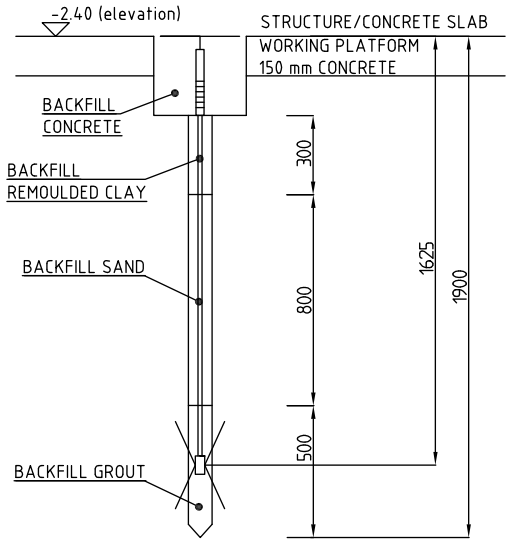

Figure C.21: *Cross section of extensometer installation in ∅90 mm hole.*

C.4 Detailed working order and photos from installation of VW sensors

A detailed working order for the installation of the sensors under the permanent concrete structure was decided on and followed step-by-step during the installations. The working order was based on two trial installations performed before the excavation reached the section to be instrumented. The trial installations resulted in the following decisions regarding the final installations:

- The cells intended for monitoring of vertical earth pressure need to be placed on a thin layer of levelling sand (fraction 0-4 mm). This in order to ensure full contact with the cell membrane. In order to eliminate potential arching effects due to sand, several attempts were made initially to place the cell directly onto a flat clay surface. However, in none of these trials such a perfectly flat surface could be prepared such that the entire cell was in contact with the clay.
- The installation of the cells intended for monitoring of horizontal earth pressure needed special consideration. A device with a point blade was constructed in order to create a pre-made trench that the earth pressure cell could be pushed into. Further, a device was constructed in order to push down the earth pressure cell without pushing or damaging the steel tube connecting the cell with the sensor housing. The devices can be seen in Figure C.22 a) and b). It was finally decided to make the trench by pressing a 8 mm thick pointy blade made out of acrylic glass (plexiglass) into the clay. This resulted in the desired combination of a) the earth pressure cell was able to be pushed down by hand and bodyweight b) full contact

between the earth pressure cell and clay interface (photo in Figure C.22 c). Based on Massarsch (1975) soil disturbance due to this installation procedure was expected to dissipate (relaxation to σ'_{h0}) rather quickly, within approximately 1 week. Two other options were tested but discarded: 1) creating the trench by pressing a 4 mm thick pointy blade made out of steel, this was discarded as during installation of the cell gaps were formed between the cell and the clay along the top part of the earth pressure cell 2) dig a 10 mm trench using a 10 mm flat iron, this resulted in very rough trench walls which were not in 100 % contact with the earth pressure cell.

The final working order and installation procedure is presented in the following including reference to photos in Figures C.22 and C.23.

1. Excavation to final depth in the studied section. Excavation was carried out sequentially and finalized on June 26$^{\text{th}}$ in the studied section.
2. Placing of well rings at three locations on the excavation bottom. Before placing of the well rings, plastic film and geotextile was placed on the excavated clay surface in order to prevent drying or wetting of the clay (due to rain). The well rings were jacked at one location of the wall in order to pull trough a *varnothing*50 mm plastic pipe for the sensor cables.
3. Placing of plastic pipes on the excavation bottom from the well rings to the future data logger location. The pipes were pre-drawn with a string in order to run extract the cables after installation of the sensors.
4. Adjustment/levelling of the excavation bottom with macadam in preparation for the pouring of the working platform concrete.
5. Casting of the concrete working platform in the studied section and around the well rings (carried out on June 27$^{\text{th}}$).
6. Installation of total earth pressure cells and piezometers within the slots/holes of the well rings. Starting with the instruments located within the well ring located closest to the west SPW, then the middle and finally the easternmost location. The working order which was repeated at all locations is given below:

    (a) Pull sensor cables (ordered in full length to avoid splicing) trough the pre-drawn plastic pipes (cast in the working platform) to the data logger location. Also pull them through protective flexible plastic pipes in order to avoid casting them into concrete and allow for slack. Connect sensor cables to logger and take site zero-readings.

    (b) Cut plastic film and geotextile previously placed to protect the clay surface.

    (c) Remove ca 2-3 cm of the top clay layer in order to expose a fresh clay surface. Dig in slightly underneath the well rings (to secure the concrete plugg that is later to be poured into the well rings from "popping up" due to heave or water pressure).

    (d) Dig a vertical cut into the clay (ca 30 cm x 10 cm wide and ca 50 cm deep) by

hand using masonry tools. Remould the excavated clay in order to use it as backfill material.

(e) In the bottom of the cut; make a trench for the cell intended to measure the horisontal stress by pressing down a 8 mm pointy blade, see Figure C.22 f).

(f) Install the earth pressure cell in the trench. Based on trial installations the trench walls and earth pressure cell were sprayed with water before installation. The cells were installed with the sensitive side (raised surface) facing the SPWs. In the approximate centerline location, the sensitive side face the west SPW.

(g) Use a ∅16 mm drillbit to make a 80 mm hole into the side of the vertical cut. Install piezometer slowly while monitoring the pressure (in order to avoid over-range pressures). See Figure C.22 g) and h) for installed horisontal earth pressure cell and piezometer.

(h) Backfill the vertical cut with remoulded clay.

(i) Carefully dig a circular hole 30 mm deep for the cell intended to measure the vertical stress. Level the excavated hole with 10 mm sand (fraction 0-4 mm). Figure C.23 a) and b).

(j) Place the cell with the sensitive side down and press gently to ensure full contact. Place a layer of plastic film on top of the cell (to prevent mortar to reach the cell and sand). Figure C.23 c) to e).

(k) Fill with 10 mm sand on top of the cell (up to the surrounding clay surface). Wet the sand by spraying water and carefully hand compact it. Place another layer of plastic film on top of the sand and seal with remoulded clay. Place geotextile on top of plastic film in order to prevent steel fibres in concrete to puncture plastic. Figure C.23 f) and g).

7. Cast concrete within well rings and on top of instruments. Pour carefully (by shovel) in order to avoid instruments to come out of position or tilt and/or puncture the plastic films. Figure C.23 h) and i).

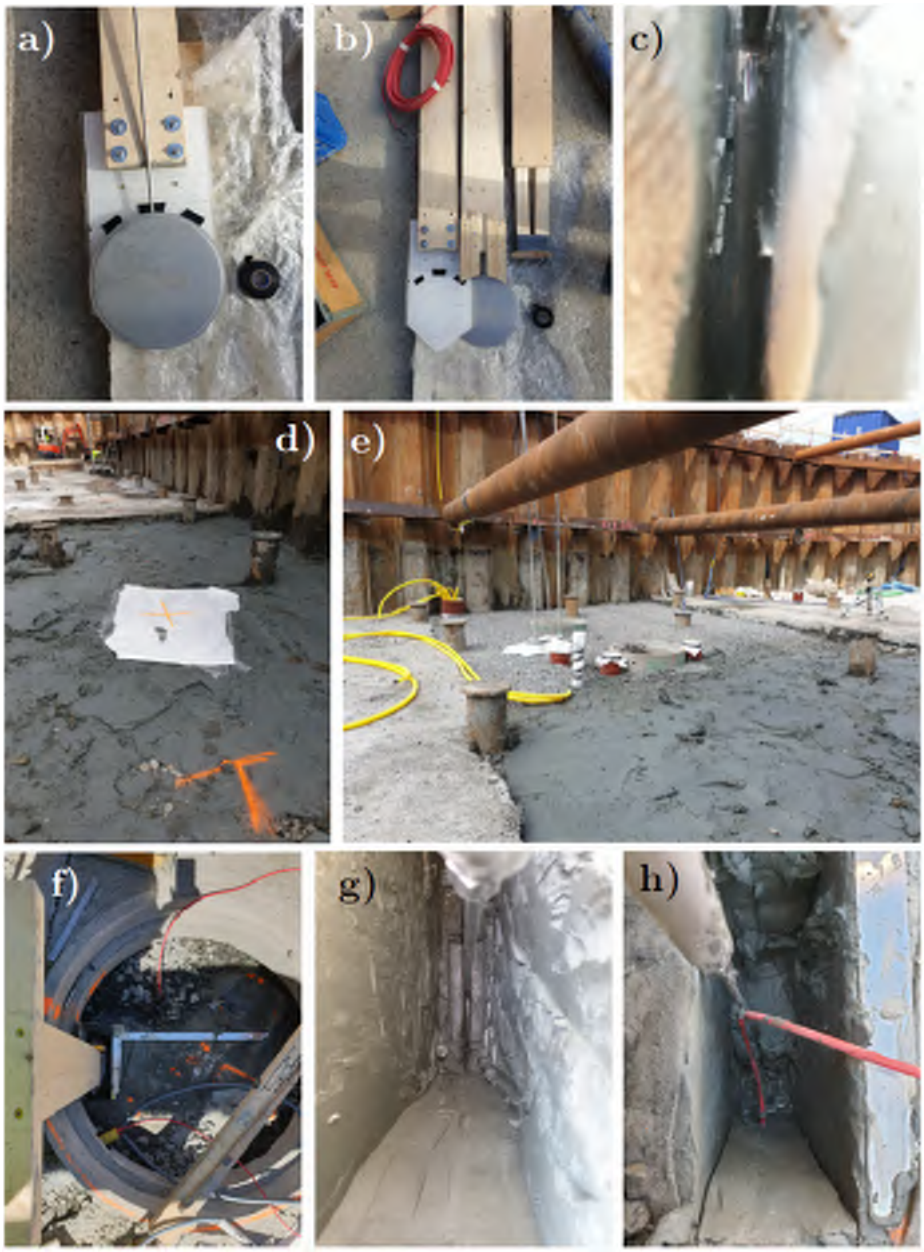

Figure C.22: *Photos from installation of horisontal earth pressure cells and piezometers including devices to install cells.*

Figure C.23: *Photos from installation of vertical earth pressure cells including final pouring of concrete over instruments.*

The working order for the installation of the extensometer is described in the following.

1. Place a ∅30 cm PVC pipe on the excavation bottom once the excavation has reached the final depth. Run a plastic pipe from the pipe to the location of the logger.
2. Cast working platform around the PVC pipe.
3. Assemble extensometer at site and run cable trough plastic pipe to data logger location.
4. Extract a ∅90 mm and 2 m deep hole in the clay. This was easily done in intervals of 30 cm with an extended garden auger. Remould the excavated clay in order to use it as backfill material.
5. Insert the extensometer with anchor spider legs in retracted position. Secure the extensometer so that it is in the correct level.
6. Pull release line to deploy spider legs.
7. Grout the hole at the depth of the spider legs anchor.
8. Backfill with sand and then, at the depth where able to reach down, backfill with remoulded clay.
9. Cast the top of the extensometer into the concrete working platform.
10. Drill a anchor rod into the concrete working platform and cast it into the bottom slab.

C.5 Table summarising the construction sequence

A summary of the main construction stages including the installations of vibrating wire sensors is given in Table C.4. For details of the construction sequence refer to the report section 4.2.4 and for the installation of VW sensors section 4.4.7.

Table C.4: Summary of main construction stages and VW sensor installations.

No.	Description	Start	Finished	Note
01	Preparatory works including pre-excavation to level +2.3	2018-09	2018-12	
02	Installation of displacement piles including pre-augering	2019-01-09	2019-02-01	Passing section 2019-01-21–25
03	Installation of SPWs	2019-02-07	2019-02-27	Passing section 2019-02-13
04	Installation top waler beam and strut level (+3)	mid March	2019-04-09	
05	Excavation for and installation of lower west waler beam level	begin. April	-	Passing section 2019-04-17
06	Excavation for lower east waler beam and strut level (±0)	begin. April	2019-05-08	Passing section 2019-05-02–03
07	Installation of east waler beam	begin. May	2019-05-24	
08	Installation of lower strut level	2019-05-27	begin. June	N to S
09	Sequential excavation (N to S) incl. casting of working platform	2019-05-29	begin. July	In section 2019-06-25–27
10	Installation VW sensors in clay (hori. TP cells and piezometers)	2019-06-28	2019-06-30	No inst. on 29$^{\text{th}}$
11	Installation VW sensors in clay (vert. TP cells)	2019-07-01	2019-07-02	
12	Cast concrete over VW sensors and install. of VW extensometer	2019-07-02	2019-07-02	
13	Cut BAT-piezometer pipes and re-route cables	2019-07-03	2019-07-03	
14	Cut lower level struts located next to section	2019-07-04	2019-07-05	
15	Rebar and form works	2019-08-13	2019-09-24	
16	Casting of slab part 1	2019-09-10	2019-09-10	Layout Fig. 4.8
17	Casting of slab part 2	2019-09-25	2019-09-25	———
18	Casting of walls	2019-10-24	2020-02-28	———
19	Back fill west wall-SPW	2019-02-26	2020-02-28	
20	Pile inst. Hisings bridge supp. 2:3	2020-03-06	2020-03-24	[1)]
21	Removal of top waler beam level	2020-03-09	2020-04-03	
22	Pile inst. Hisings bridge supp. 2:2	2020-03-30	2020-04-08	[2)]
23	Pre-drilling for piles S of tunnel	2020-04-30,-05-04/	-05/-06	[3)]
24	Casting North ($1/4^{th}$) of roof	2020-05-15	2020-05-15	94 m^3

[1)] 8 hammered steel piles, top 24 m ∅610 mm on 54 m ∅406 mm, pre-augering to 18 m depth, ≈100 m North of location of WV sensors. [2)] 8 piles as above but support ≈60 m North of VW sensors. [3)] To 6 m depth BGS, air hammer through fill. 2020-04-30 3 locations within SPWs 1 location -05-04.

C.6 Measurement data not presented in the report

This section covers measurement data not included in the report.

C.6.1 Pore pressure during piling and excavation works

The pore pressure measured in the BAT piezometers during the piling and excavation works is presented in Figure C.24. Assumed stationary pore pressures before constructions works have been included in the figure. The BAT piezometers were located inside the excavation and approximately 1.5 m west of the West SPW (for location see Figure 4.22).

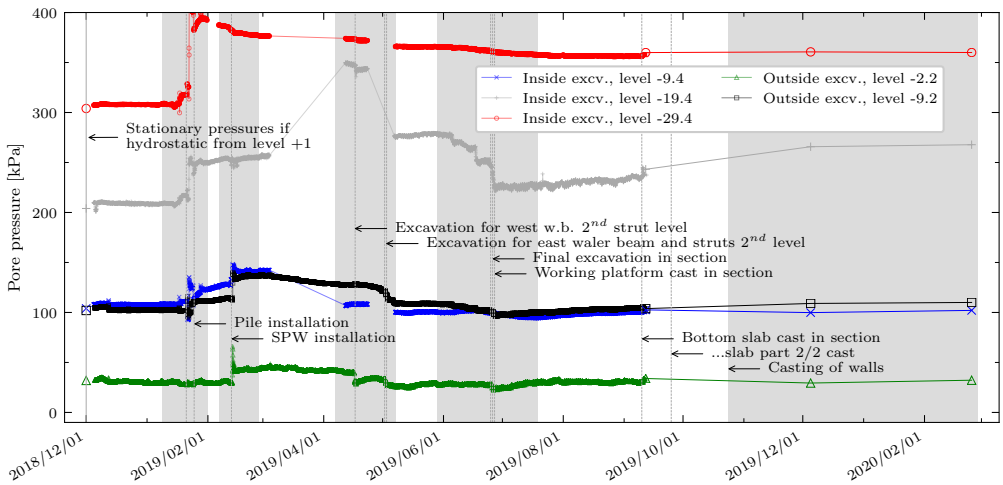

Figure C.24: *Pore pressures measured in the BAT piezometers inside and outside the excavation.*

C.6.2 Total stresses and pore pressure under slab

Figures C.25 covers compilation of measurement data from each of the three locations with sensors installed under the concrete slab. In these plots measurements of pore pressure and total stresses are corrected for changes in barometric pressure and temperature. Temperature correction for total earth pressure cells is presented as both corrected for CFT_{vw} only (as presented in the figures in the report) and corrected for CFT_{vw}+CFT_{cell} with a value of CFT_{cell}=0.2 kPa/°C. As the thermistors are located in the VW transducer housings, the CFT_{cell} for the horizontal earth pressure has been multiplied with the temperature reading from the piezometers (as these are located nearer/deeper the horizontal membrane than the thermistor in the TP-cell). Earth pressure cell readings are also presented as completely uncorrected with respect to temperature variation. This illustrates the effect on considering temperature correction, as e.g. peak values in stress during temperature increase are reduced. The occurrence of main construction stages including casting order for the walls of the structure are annotated. For layout of wall locations refer to Figure 4.8. Note that the effective stress has not been adjusted for

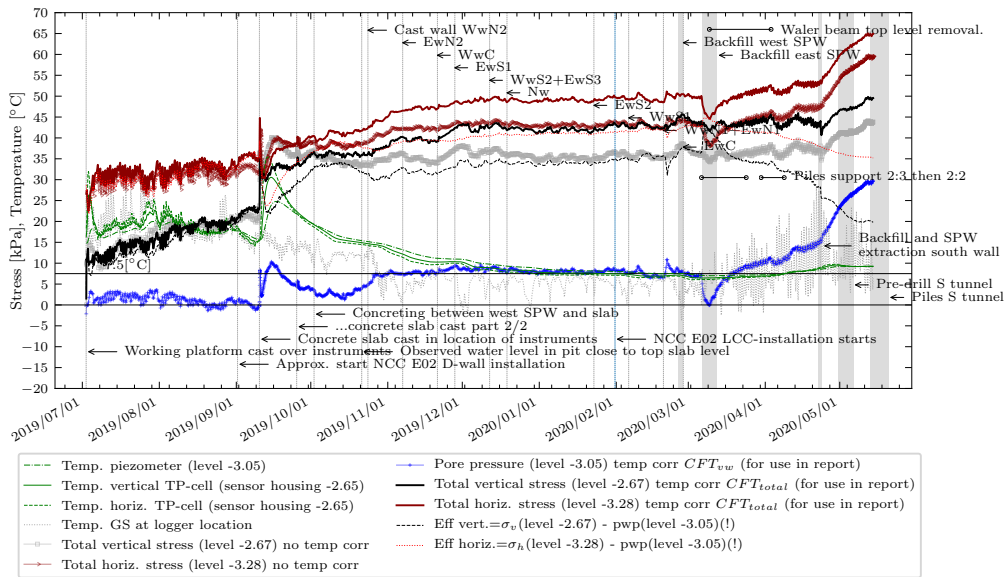

Figure C.25: *Compilation of measurement data obtained from location closest to west SPW including evaluation of effective stresses.*

Uncorrected measurement data from vibrating wire total earth pressure cells installed in the clay under the permanent structure are presented in Figure C.28. These data have *not* been corrected for change in barometric pressure or temperature. The influence of the barometric pressure changes on the total stress readings is seen as the data sets clearly are correlated to the barometric pressure change. The same holds for the piezometer data. Corrected data on total stresses and pore pressure with respect to change in both

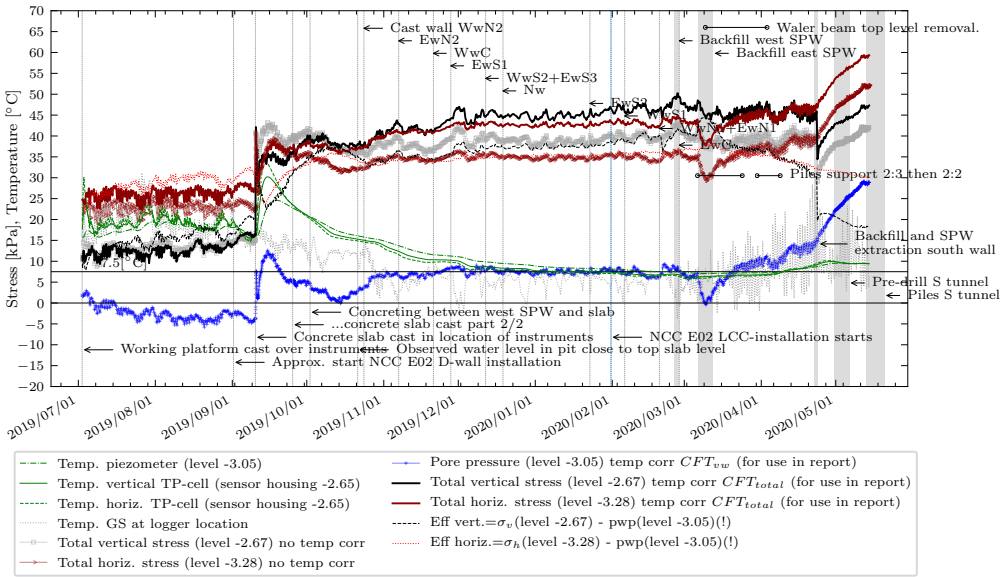

Figure C.26: *Compilation of measurement data from centremost location of excavation including evaluation of effective stresses.*

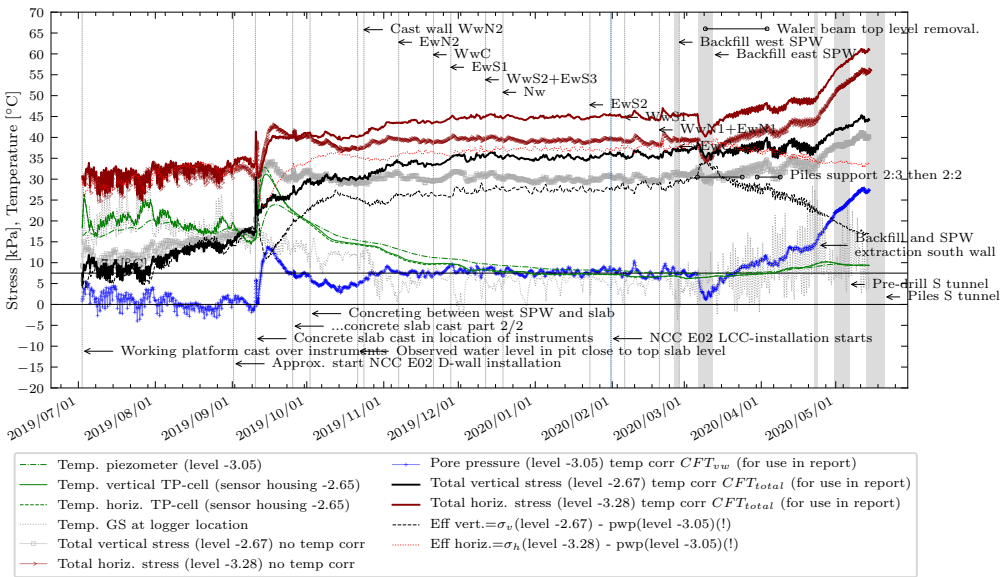

Figure C.27: *Compilation of measurement data obtained from location closest to east SPW including evaluation of effective stresses.*

barometric pressure and temperature are presented in the report in Figures 5.8 and 5.7.

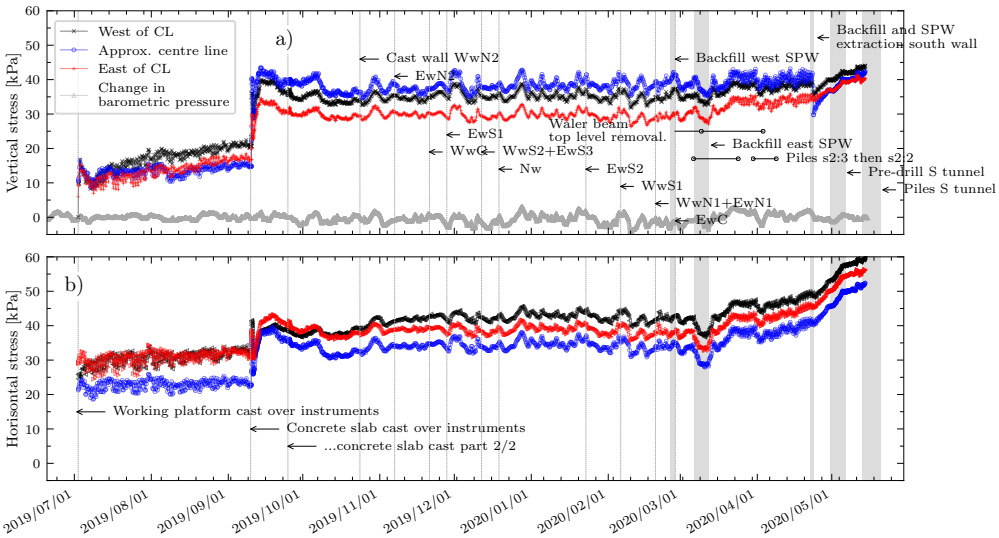

Figure C.28: *Registered total stresses under concrete slab, a) vertical and b) horizontal pressures. Measurement data* ***not*** *corrected for changes in barometric pressure or temperature. The change in barometric pressure with reference to 2019-07-02 13:00 (101.2 kPa at the time when casting the working platform over the instruments) is included based on data from Swedish Meteorological and Hydrological Institute (2020a).*